



# Mechanochemical construction of mesoporous silicon-supported organocatalysts with alkylol-amine cooperative sites for CO<sub>2</sub> fixation into cyclic carbonates under halogen-free conditions

Cheng Li<sup>a,1</sup>, Wenjie Xiong<sup>b,1</sup>, Tianxiang Zhao<sup>a,\*</sup>, Fei Liu<sup>a,\*</sup>, Hesun Cai<sup>a</sup>, Peng Chen<sup>a</sup>, Xingbang Hu<sup>b,\*</sup>

<sup>a</sup> Key Laboratory of Green Chemical and Clean Energy Technology, School of Chemistry and Chemical Engineering, Guizhou University, Guiyang 550025, PR China

<sup>b</sup> School of Chemistry and Chemical Engineering, Nanjing University, Nanjing, Jiangsu 210093, PR China

## ARTICLE INFO

### Keywords:

CO<sub>2</sub>  
Cyclic carbonate  
Mechanochemical  
Halogen-free  
Organocatalyst

## ABSTRACT

In this work, we demonstrated a mechanochemical method to quickly fabricate mesoporous SiO<sub>2</sub>-supported organocatalysts with alkylol-amine cooperative sites. The detailed characterizations of solid-state NMR, FTIR, XPS, TGA, as well as electron microscope confirmed that the organocatalysts were successfully grafted on the surface of SiO<sub>2</sub> by mechanically ball-milling without any solvent. These SiO<sub>2</sub>-supported organocatalysts exhibit medium to remarkable activity for the cycloaddition of CO<sub>2</sub> and epoxides under halogen- and solvent-free conditions, and the activity of the catalysts can be also adjusted by controlling the pore size of the support SiO<sub>2</sub> and the structure of organocatalysts. Further mechanistic studies suggest that the good activity originates from the synergistic effect between the alkylol and amine sites. Furthermore, SiO<sub>2</sub>-supported organocatalysts can be easily recovered and recycled. This work not only provides an efficient method for the agile construction of multifunctional organic-inorganic hybrid materials, but also provides an alternative halogen-free catalyst for CO<sub>2</sub> conversion.

## 1. Introduction

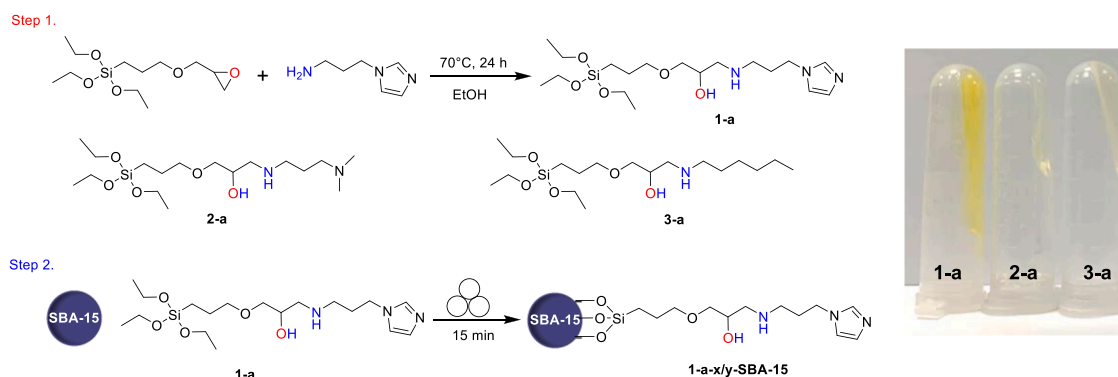
Since industrialization, excessive emission of carbon dioxide (CO<sub>2</sub>) has become a major environmental problem [1]. In order to reduce the greenhouse gases CO<sub>2</sub> concentration in the atmosphere and promote the sustainable development of resources and environment, the development of effective CO<sub>2</sub> capture and utilization technologies is a proven approach. Considering that CO<sub>2</sub> is also an abundant, non-toxic, and recyclable C1 resource, chemically fixed of CO<sub>2</sub> in high value-added products and fuels is highly desirable to reduce the negative environmental impacts [2]. However, CO<sub>2</sub> utilization is challenging due to the thermodynamic and kinetic limitations of inert CO<sub>2</sub> [3]. Among them, CO<sub>2</sub> cycloaddition to synthesize cyclic carbonates is very attractive, which has the characteristics of simple synthesis and cost-effectiveness. And cyclic carbonates are highly precious materials in industrial applications due to properties such as high dipole moment, boiling point, stability, low toxicity, and biodegradability [4,5]. The synthesis of cyclic carbonates has attracted much attention in the field of catalysis.

Many homogeneous and heterogeneous catalysts have been widely reported, such as organometallic compounds [6,7], metal-organic frameworks (MOFs) [8,9], zeolitic imidazolate frameworks [10], ionic liquids [11,12], organocatalysts [13], hybrid organic-inorganic materials [14,15], and so on. Yang et al. reported a cationic Zn(II)-porphyrin immobilized silica as an effective catalyst for the cycloaddition of CO<sub>2</sub> and epoxides without any cocatalysts [7], in which Lewis acid and Br<sup>-</sup> of metal-based catalysts can synergistically enhance the catalytic activity for CO<sub>2</sub> cycloaddition reaction. Based on a similar mechanism, Sun et al. reported a bimetallic MOFs catalyst (Zn/Mg-MOF-74) [8], relying on unsaturated metal centers as active Lewis acid sites and terbutylammonium bromide as a cocatalyst, the yield and selectivity of the cyclic carbonates are both up to 99%. The halogen-containing cocatalysts in these catalytic protocols are essential to obtain satisfactory conversion of epoxides, but this undoubtedly reduces the greenness of the reaction process due to the strong corrosiveness and toxicity of halide ions [16,17]. Moreover, residues of halogens and metals also greatly affect the purification of products. It is imperative to design

\* Corresponding authors.

E-mail addresses: [txzhao3@gzu.edu.cn](mailto:txzhao3@gzu.edu.cn) (T. Zhao), [ce.feiliu@gzu.edu.cn](mailto:ce.feiliu@gzu.edu.cn) (F. Liu), [huxb@nju.edu.cn](mailto:huxb@nju.edu.cn) (X. Hu).

<sup>1</sup> C. Li and W.J. Xiong contributed equally to this work.



**Scheme 1.** Schematic illustration of the immobilized organocatalysts on SBA-15 and image of silane **n-a** (placed upside down).

efficient metal- and halide-free catalysts to achieve green and sustainable strategies for CO<sub>2</sub> cycloaddition.

In the past few decades, hybrid organic-inorganic materials have become a research hotspot in heterogeneous catalytic CO<sub>2</sub> fixation into cyclic carbonates, especially those silicon-based catalysts. Back in 2009, Park et al. [14] obtained a stable heterogeneous catalyst for CO<sub>2</sub> conversion by grafting ionic liquids onto commercial silica. A variety of similar hybrid organic-inorganic catalysts were subsequently proposed [15,18–21]. For instance, Zhang et al. reported a series of SBA-15 supported triazolium-based ionic liquids hybrid materials [15]. It was found that high yields (80–99%) and excellent selectivity (97–99%) of cyclic carbonates could be achieved under mild conditions without additional organic solvents or co-catalysts. Hereafter, carboxylic acid functionalized SBA-15 was fabricated by Islam et al., without any halogen atoms [18], which showed suitable catalytic activity for the production of cyclic carbonates with the help of a cocatalyst at atmospheric pressure and room temperature. The traditional method for the preparation of SiO<sub>2</sub>-based hybrid organic-inorganic materials is that a silane coupling agent is covalently bonded to SiO<sub>2</sub>, which needs to suffer from high temperature, large amounts of solvent toluene, as well as a long reaction time. How to optimize the above tedious synthetic routes will be of great significance to the construction of this type of hybrid materials. A mechanochemical method for the synthesis of hybrid organic-inorganic materials, completing chemical grafting at room temperature under solvent-less conditions, was developed in 2020 by Amrute et al. [22]. Silane coupling agent can be covalently grafted on the surface of SiO<sub>2</sub> through hydrolysis and condensation, induced by the mechanical force of ball milling [23]. Many works have shown that mechanochemical synthesis offers a versatile, simple, high-efficiency, and solvent-free alternative to the solvothermal route for constructing catalytic materials [24,25]. The distinctive advantages of mechanochemically process are operated without a need for additives (e.g., solvents, templates) and post-synthetic treatments. This avoids the generation of solvent and simplifies the entire synthesis path, ultimately simplifying scale-up. Moreover, several of these systems have shown better performance in various catalytic applications [26–28]. However, there are few works on the structural regulation of SiO<sub>2</sub>-based hybrid organic-inorganic materials due to the multi-factor influence of the structure. Moreover, the structure-activity relationship between material structure and properties is not clear in the previous reports.

Herein, combined with the design of a halogen-free catalyst for CO<sub>2</sub> cycloaddition, we demonstrated a mechanochemical method for the rapid construction of mesoporous silicon-supported organocatalysts for CO<sub>2</sub> fixation into cyclic carbonates. These organocatalysts with alkylol-amine cooperative sites were first synthesized by a ring-opening reaction of epoxy and primary amine and subsequently covalently grafted onto SBA-15 within 15 min via a mechanochemical method without any solvent. Taking CO<sub>2</sub> cycloaddition as a model reaction, the relationship between the structure and performance of these SiO<sub>2</sub>-based hybrid

catalysts was systematically studied through experiments and theoretical calculations. The facile preparation method, considerable catalytic activity, and good stability of the SiO<sub>2</sub>-based hybrid organic-inorganic materials confirm the applicability and advancement of mechanochemical construction of hybrid catalytic materials.

## 2. Experimental section

### 2.1. Materials

Tetraethyl orthosilicate (TEOS, 98%, Aladdin chemistry, China), hydrochloric acid (36%–38%), triblock copolymer P123 (Sigma-Aldrich, China). (3-glycidyloxypropyl)triethoxysilane (96%), N-(3-aminopropyl)-imidazole (98%), 3-dimethylaminopropylamine (99%), n-heptyl-amine (98%), hexylamine (99%) were purchased from Adamas Reagent Co., Ltd. Other chemicals (analytic grade) were purchased from Energy Chemical Technology (Shanghai) Co., Ltd. All reagents were utilized as received without further purification. CO<sub>2</sub> (>99.99%) and N<sub>2</sub> (>99.999%) were supplied by Guiyang Sanhe Special Gas Center, China.

### 2.2. Preparation of SBA-15

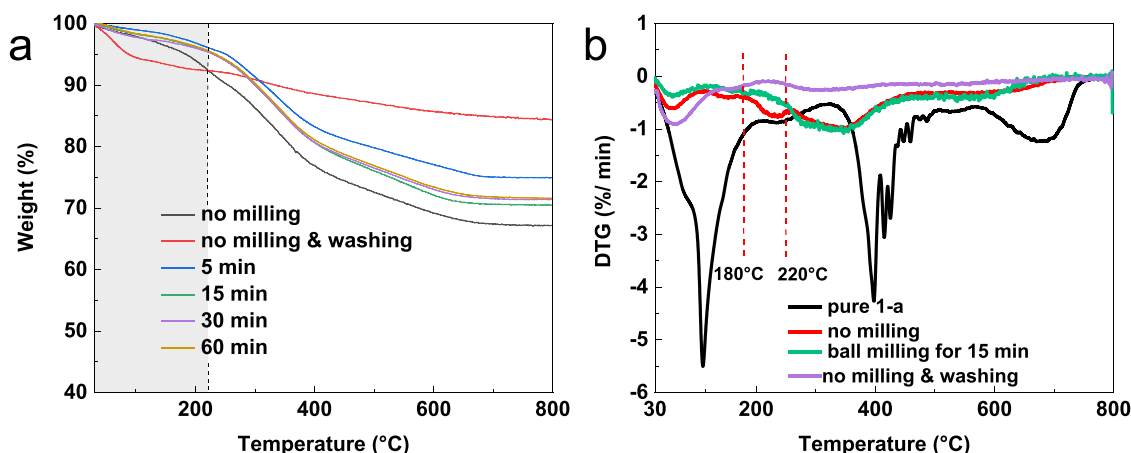
SBA-15 was prepared according to methods reported in the literature [29]. Firstly, P123 (2 g) was dissolved in concentrated HCl (10 mL) and distilled water (53 mL) in a 500 mL beaker. The solution was stirred for 3 h at room temperature. TEOS (3.853 g) was added dropwise to the solution, and the mixture was subsequently stirred for 21 h at 40 °C and then heated at 100 °C for another 24 h under static conditions. Afterwards, the mesoporous material was filtered with copious amounts of distilled water, and the resulting white powder was then dried in an oven at 60 °C. Finally, the powder was calcined at 550 °C for 6 h, and cooled to room temperature, then we got b-SBA-15. To obtain the SBA-15 with different pore size structures, the a-SBA-15 (70 °C) and c-SBA-15 (130 °C) were synthesized by the same method but at different hydrothermal reaction temperatures.

### 2.3. Preparation of SBA-15 supported organocatalysts (n-a-x/y-SBA-15)

The synthesis of n-a-x/y-SBA-15 in this work was mainly parted into two processes, as shown in Scheme 1.

**Step 1:** Organocatalysts as the silanes were synthesized by a ring-opening reaction of primary amine and epoxy groups [30,31]. Typically, 2 mmol of (3-glycidyloxypropyl)triethoxysilane and 2 mmol of N-(3-aminopropyl)-imidazole were added to 8 mL ethanol and then heated at 70 °C for 24 h. Then the ethanol was removed by vacuum drying at 40 °C. The organocatalysts obtained as the highly viscous liquids were marked as **n-a**, and their structures were characterized by <sup>1</sup>H NMR and shown in Figs. S1–3.

**Step 2:** The immobilized organocatalysts were synthesized via a



**Fig. 1.** (a) TGA curves of 1-a-40/b-SBA-15 with different ball milling time. (b) DTG curves of pure 1-a, 1-a-40/b-SBA-15, and physically mixed 1-a-40 and b-SBA-15 before (no milling) and after washing with ethanol (no milling & washing).

mechanochemical grafting method [22]. Typically, 0.4 g of b-SBA-15 and 0.6 g of 1-a were mixed in a 45 mL of ZrO<sub>2</sub> grinding bowl with 20 zirconium oxide balls ( $d = 10$  mm, 70 g). The mixture was reacted by ball milling at room temperature for 15 min using a vertical planetary mill (YXQM-0.4 L, MITR Instrument & Equipment Co., Ltd., China) at the rotational speed of 500 rpm. The immobilized organocatalyst was repeatedly washed with methanol and ethanol to remove ungrafted silane. After vacuum drying at 60 °C for 24 h, the immobilized organocatalyst was obtained with a theoretical loading of 60 wt%, marked as 1-a-60/b-SBA-15. Other catalysts (n-a-x/y-SBA-15, where n-a represents different silanes, x represents the dosage of silane during ball milling, and y represents silicon dioxide with different pore diameters) were prepared in a similar way but differed in the dosage and structure of organocatalysts and SBA-15. As a control, the physically mixed 1-a-40/b-SBA-15 was ground manually for 15 min instead of ball milling based on the same feeding amount. It was repeatedly washed with ethanol to remove ungrafted silane (marked as no milling & washing).

#### 2.4. Catalyst characterization

Powder X-ray diffraction (XRD) was measured using a Small-angle X-ray diffractometer (D8 advance) applying Cu K $\alpha$  as the irradiation source at 40 kV and 40 mA. Data were recorded in the 0.5–3° (for the detection of reflection of ordered mesoporous materials) or 5–90° 2 $\theta$  range. Fourier transform infrared (FTIR) spectra of catalysts that were used for confirming structures were recorded on Nicolet iS50 FTIR spectrometer with anhydrous KBr as the standard. FTIR spectra in the diffuse reflectance (DRIFTS) mode were recorded on a Nicolet iS50 using a mercury cadmium telluride (MCT) detector. Thermogravimetric analysis (TGA) was carried out by STA 449F5 simultaneous thermal analyzer. The heating program was set as rising to 800 °C at a rate of 10 °C min<sup>-1</sup>. Analyses were performed in O<sub>2</sub> (50 cm<sup>3</sup> STP min<sup>-1</sup>). The morphology and porous structure were analyzed by scanning electron microscope (SEM, Quanta FEG 650) and transmission electron microscope (TEM, FEI G2 F20). The surface chemical compositions of samples were studied by X-ray photoelectron spectra (XPS). Data were collected at a K-Alpha Plus photoelectron spectrometer utilizing monochromated Al K $\alpha$  (1500 eV) irradiation. Nitrogen adsorption isotherms of various samples were measured with a BSD-PS(M) surface area and porosity analyzer (Beishide Instrument-S&T) at -196 °C. Prior to implementing the measurements, the samples were degassed at 120 °C for 6 h. <sup>29</sup>Si MAS NMR and <sup>13</sup>C MAS NMR spectra were recorded on a Bruker Biospin GmbH 400 MHz spectrometer using a double-bearing standard MAS probe (DVT BL4) operating at a resonance frequency of 99.4 MHz. <sup>1</sup>H NMR spectra were recorded on a JNM-ECZ-400 spectrometer operating at 400 MHz with CDCl<sub>3</sub> as the solvent. The yield and selectivity were

determined via GC system (SHIMADZU GC-2014 C) with a FID detector.

#### 2.5. Catalytic evaluation

The cycloaddition of CO<sub>2</sub> and epoxides was carried out according to our recent method with slight modifications [32]. Firstly, 10 mmol of styrene oxide (SO) and 1 mol% of catalyst (based on organocatalyst) were added into a 50 mL stainless-steel autoclave with a magnetic stirrer. Then, after purging the autoclave with CO<sub>2</sub> for three times, the reactor was pressurized to 1.0 MPa of CO<sub>2</sub>. Finally, reacting at 120 °C for 12 h with a stir speed of 300 rpm, the reactor was cooled to room temperature. The mixture was diluted with ethyl acetate for quantitative analysis with gas chromatography. For catalyst recycling, the residue solid catalyst was recovered by centrifugation after the reaction, then washed with ethyl acetate and ethanol, and dried in a vacuum at 60 °C for 12 h. After that, the catalyst is charged into the next reaction under the same reaction conditions. To test the stability of the catalyst, a leaching test experiment was conducted. After 6 h of reaction, the solid catalyst was separated from the hot reaction solution by centrifugation (rotational speed of 12,000 rpm for 10 min). The reaction was continued with the filtrate in the absence of catalyst for an additional 6 h.

#### 2.6. Theoretical calculation method

All the structures were fully optimized with the B3LYP method based on DFT including the dispersion corrections using the Empirical Dispersion = GD3BJ keyword. 6–31 g(d) basis set was used to optimize for all atoms [abbreviation as B3LYP/6–31 g(d)] [33–36]. Furthermore, for more precision, a single-point energy was calculated for the energy profile by using the Polarizable Continuum Model (PCM) with the effect of methanol solvent on the condensed phase at the B3LYP/6–311++g(d,p) level. Energy calculations and Zero-point energy (ZPE) correction have been done by using the same level of theory. The computed stationary points have been characterized as minima or transition states by diagonalizing the Hessian matrix and analyzing the vibrational normal modes. In this way, if the imaginary frequency is not displayed, the stationary point can be classified as minima, and if only one imaginary frequency is obtained, the stationary point can be classified as a transition state (TS). The particular nature of the transition states has been determined by analyzing the motion described by the eigenvector associated with the imaginary frequency. All calculations were performed with the Gaussian 09 suite of programs [37].

### 3. Results and discussion

#### 3.1. Catalyst synthesis and structure characterization

##### 3.1.1. Mechanochemical synthesis of SBA-15 supported organocatalysts

All SBA-15 supported organocatalysts were fabricated via a mechanochemical approach. The effect of ball milling time on catalyst structure was first investigated by using b-SBA-15 as support and 40 wt% organocatalyst **1-a** as silylation. The efficiency of silylation was determined by TGA and DTG curves that are shown in Fig. 1, and the weight loss of 1-a-40/b-SBA-15 above 220 °C was defined as the effective grafting amount of **1-a**.

As shown in Fig. 1a, the weight loss for 5, 15, 30, and 60 min milling periods demonstrated a similar weightlessness trend, among which 15 min of ball milling was sufficient to achieve optimum loading of the **1-a** with a 62.5% efficiency of silylation (see Table 1, entry 2). Although the ball milling time was prolonged, the grafting amount did not increase, which may be related to the richness of surface hydroxyls [22, 38]. Notably, the grafted catalyst 1-a-40/b-SBA-15 was the most stable with an initial mass loss higher than 220 °C, suggesting that the chemical grafting can be accomplished by mechanical ball milling under solvent-free conditions (entries 1–4). In contrast, physically mixed 1-a-40/b-SBA-15 showed poor thermal stability but higher than pure **1-a** (Fig. 1b), possibly due to the hydrogen bonding interaction between the silica and **1-a**. Subsequently, the physically mixed 1-a-40/b-SBA-15 was washed with ethanol for many times to remove the ungrafted **1-a**. It was still found that about 6.9% of **1-a** is chemically grafted onto the surface of silica (entry 6). In addition, by changing the ball milling dosage of silane, a series of SBA-15 supported organocatalysts with different silica loading were fabricated (entries 7–9).

##### 3.1.2. Catalyst characterization

After clarifying the catalyst immobilization methods, the structure of b-SBA-15 supported organocatalysts with different dosages of silane during ball milling was characterized. As shown in Fig. 2a, the TGA curves showed that the first weight loss (before 100 °C) is attributed to the physical adsorption of water, and the second dramatic weight loss is attributed to the decomposition of **1-a**. Significantly, the thermal stability of the catalysts decreased gradually with the increase of the loading of **1-a**. Compared with pure **1-a**, the improved thermal stability of 1-a-x/b-SBA-15 suggested that **1-a** was grafted successfully on silica by mechanical ball milling. Most importantly, the higher decomposition temperature of the 1-a-x/b-SBA-15 ensured that it is sufficiently stable at the reaction temperature.

It can be seen from Fig. S4 that the physically mixed 1-a-40/b-SBA-15 showed only slight signature peaks for CH<sub>2</sub> groups in FTIR, proving that physically mixed 1-a-40/b-SBA-15 is difficult to form chemical bonds. On the contrary, FTIR analysis showed progressively enhanced methylene groups at 2956 and 2854 cm<sup>-1</sup>, shown in Fig. 2a, which are attributed to antisymmetric and symmetric stretching vibrations [24,

39]. Correspondingly, the bending vibration of C-H for methylene groups at 1465 cm<sup>-1</sup> also gradually appeared as the load increases of **1-a**. In addition, a methyl signal at 1407 cm<sup>-1</sup> originating from the **1-a** structure was also observed, probably due to the incomplete reaction of the ethoxy groups in the **1-a** with silica. In addition, a methyl signal at 1407 cm<sup>-1</sup> originating from the **1-a** structure was also observed, probably due to the incomplete reaction of the ethoxy groups in the **1-a** with silica. The imidazolium molecule exhibited the characteristic bands of ring stretching at 1560 and 1460 cm<sup>-1</sup>; meanwhile, an increasing N-H bond signal at 1650 cm<sup>-1</sup> clearly demonstrated the increasing organic component **1-a**. All FTIR results indicated that **1-a** can be grafted onto silica by mechanical ball milling.

The structure of the catalyst 1-a-60/b-SBA-15 was further identified by XPS. It can be seen from Fig. 2c that a new signal of N element appears in the XPS survey spectrum when **1-a** with a 60 wt% amount of milled silane was grafted on b-SBA-15 by mechanical ball milling. Accordingly, the N 1s spectrum of 1-a/b-SBA-15 emerged three peaks at binding energies of 401.4, 400.5, and 399.0 eV, as shown in Fig. 2d. These signals originated from **1-a**, which are attributed to N-H of the backbone and N-C, N=C of the imidazole ring, respectively [40,41]. In addition, the Cls spectrum of 1-a-60/b-SBA-15 also confirmed the successful introduction of N into silica through mechanochemical grafting (Fig. S5).

The nature of the chemical bonds between the **1-a** and the b-SBA-15 surface was also explored by solid-state NMR (Fig. 2e and f). The significant chemical shift at -114 ppm can be assigned as Q<sup>4</sup> [Si(OSi)<sub>4</sub>], and the chemical shift at -104 ppm can be assigned to Q<sup>3</sup> [HO-Si(OSi)<sub>3</sub>] [7,42]. Notably, a weak signal centered at -67 ppm was also observed, corresponding to the T<sup>3</sup> resonance [-CH<sub>2</sub>-Si(OSi)<sub>3</sub>], assigning to the silicon atom connected with the organic group [43,44]. The solid-state <sup>13</sup>C MAS NMR spectrum showed that all of the characteristic signals of carbons can be assigned to corresponding chemical structures of 1-a/b-SBA-15 (Fig. 2f). The spectrum also displayed the resonances signal of imidazole between 145 and 110 ppm. In addition, the weak characteristic peaks of carbonyl carbon atoms labeled by 10 were observed at about 170 ppm, which may be due to the adsorption of CO<sub>2</sub> by alkaline amine sites [45]. Based on all results, the imidazolyl silane was successfully immobilized into the b-SBA-15 by mechanical ball milling.

The morphological structure of b-SBA-15 and 1-a-60/b-SBA-15 was characterized by SEM and TEM. It can be clearly found from Fig. 3a that the b-SBA-15 is in the shape of rice grains. TEM results (Fig. 3c) showed that the b-SBA-15 has ordered regular hexagonal pore characteristics. After **1-a** was mechanochemical grafted on SBA-15, the appearance morphology of SBA-15 was retained and there was no obvious agglomeration of the organocatalyst (Fig. 3b). As shown in Fig. 3d, most of organic components **1-a** were grafted in the mesoporous, but it is undeniable that there is also **1-a** grafted on the external surface of the support. In addition, elemental mapping images of 1-a-60/b-SBA-15 also showed quite uniform dispersion of Si, O, C, and N (Fig. 3e-j), indicating

**Table 1**  
Effect of ball milling time and dosage of silane on the efficiency of silylation.

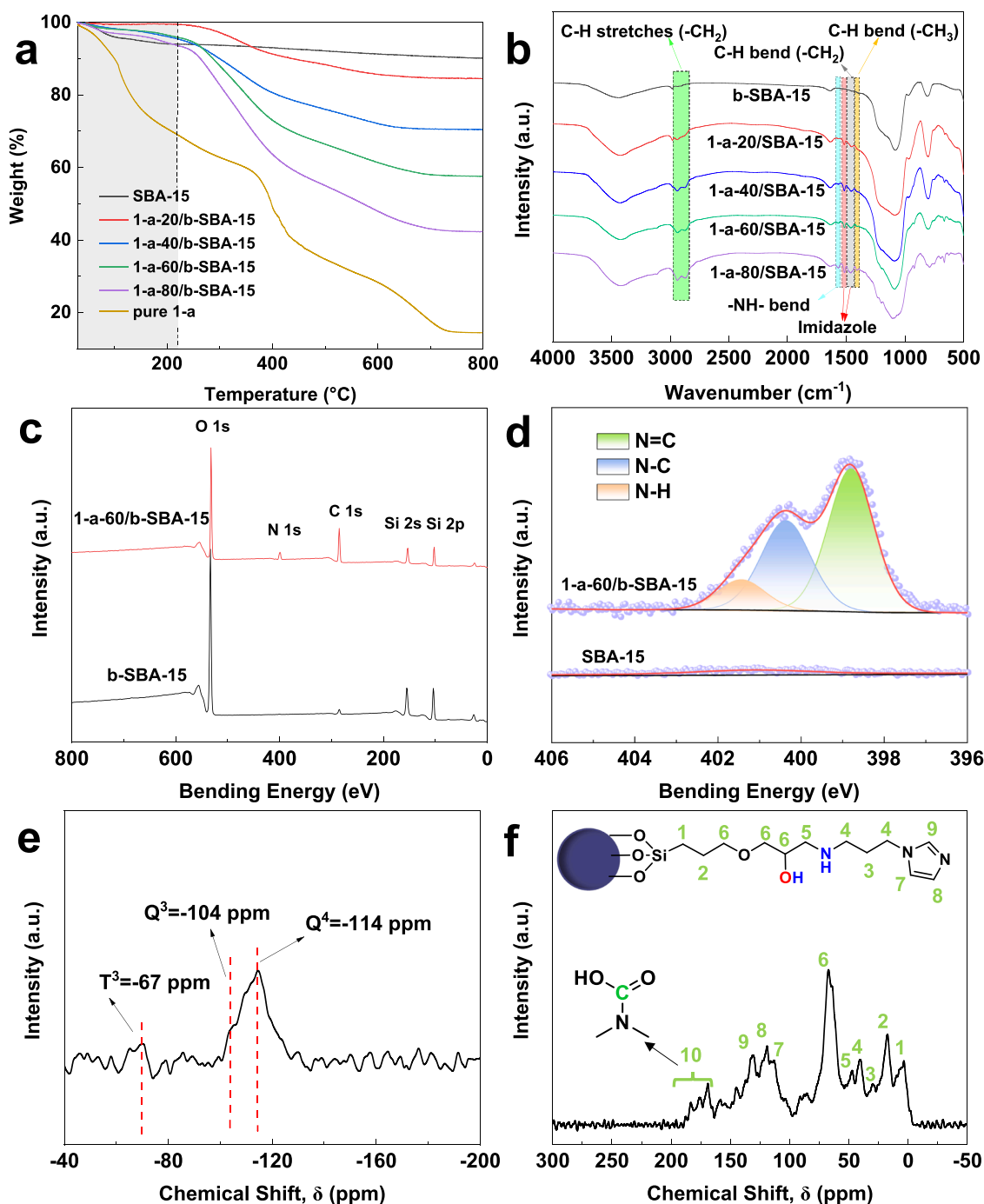
Entry	1-a-x/b-SBA-15	Ball milling time (min)	Amount of milled silane (wt%)	Amount of silylated silane (wt%) <sup>a</sup>	Efficiency of silylation (%) <sup>b</sup>
1	1-a-40/b-SBA-15	5	40	21.2	53.0
2	1-a-40/b-SBA-15	15	40	25.0	62.5
3	1-a-40/b-SBA-15	30	40	24.0	60.0
4	1-a-40/b-SBA-15	60	40	24.1	60.3
5 <sup>c</sup>	1-a-40/b-SBA-15	no milling	40	38.0	–
6	1-a-40/b-SBA-15	no milling & washing	40	6.9	17.2
7	1-a-20/b-SBA-15	15	20	15.0	75.0
8	1-a-60/b-SBA-15	15	60	38.0	63.3
9	1-a-80/b-SBA-15	15	80	51.3	64.1

<sup>a</sup> Calculated from TGA weight loss in the range of 220–800 °C for b-SBA-15 in O<sub>2</sub> atmosphere.

<sup>b</sup> Estimated from the amounts of milled and silylated silane.

<sup>c</sup> Calculated from TGA weight loss in the range of 100–800 °C for b-SBA-15 in O<sub>2</sub> atmosphere.





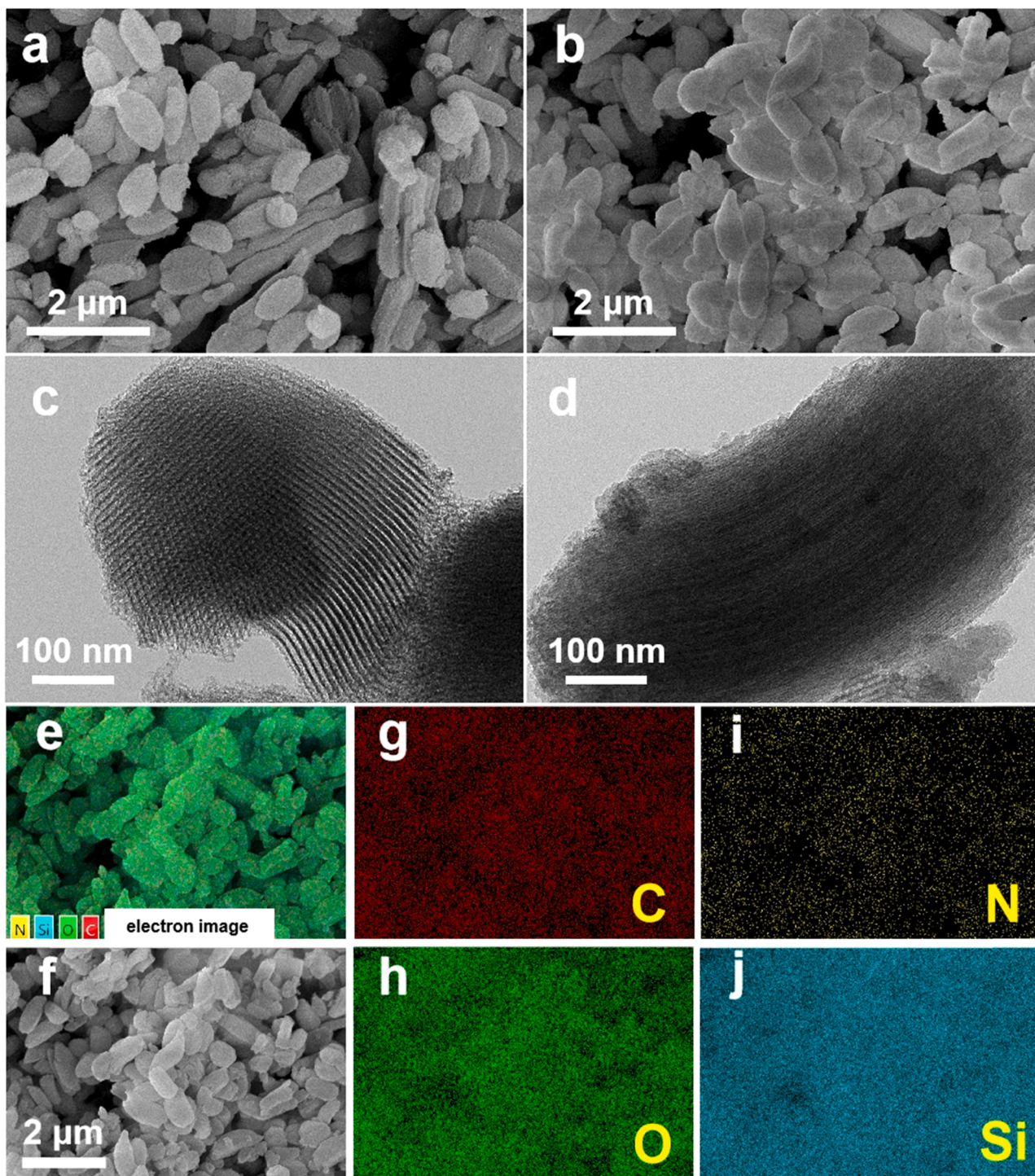
**Fig. 2.** (a) TGA weight loss profiles and (b) FTIR spectra of 1-a-x/b-SBA-15. (c) XPS survey spectra and (d) N 1s core-level spectra of 1-a-60/b-SBA-15 and b-SBA-15. (e) <sup>29</sup>Si MAS NMR and (f) <sup>13</sup>C solid-state MAS NMR spectra of 1-a-60/b-SBA-15.

imidazolyl silane was uniformly dispersed into the b-SBA-15 by mechanochemical grafting.

To further analyze the pore structural characteristics of the 1-a/b-SBA-15, XRD and N<sub>2</sub> adsorption-desorption analysis were employed. In the low-angle XRD pattern (Fig. 4a), three characteristic diffraction peaks of b-SBA-15 could be observed, attributed to the (100), (110), and (200) crystal diffraction peaks [29,46,47]. This result suggests that b-SBA-15 possesses a highly ordered hexagonal mesoporous structure. After grafting 1-a onto b-SBA-15, the crystal plane diffraction peak of (100) still remained, but the diffraction peaks of (110) and (200) gradually disappeared with the increase in grafting capacity. This is due to the fact that a number of organocatalysts were grafted into the pores

of b-SBA-15, resulting in a decrease in orderliness (Detailed diffraction peak intensity data are shown in Table S1). These results indicate that 1-a-x/b-SBA-15 still has an ordered hexagonal mesoporous structure, which is consistent with the previous TEM results. Interestingly, it can be observed in the wide-angle XRD pattern (Fig. 4b) that all the catalysts 1-a-x/b-SBA-15 only have a wide diffraction peak at 22.4°, which is a typical peak of amorphous SiO<sub>2</sub>, meaning that ball milling does not alter the intrinsic crystal structure of b-SBA-15.

The N<sub>2</sub> adsorption-desorption isotherms of 1-a-x/b-SBA-15 evidenced a type IV isotherm with H1 hysteresis loops and is characteristic of mesoporous materials (Fig. 4c) [48]. After loading of imidazolyl silane, the hysteresis loops in the medium-pressure region shifted



**Fig. 3.** SEM images of (a) b-SBA-15 and (b) 1-a-60/b-SBA-15, TEM images of (c) b-SBA-15 and (d) 1-a-60/b-SBA-15, (e–j) elemental mapping images of 1-a-60/b-SBA-15.

towards lower relative pressure with the increase of in grafting capacity, which is closely related to the filling of silane in the mesopores of b-SBA-15. Accordingly, the pore size,  $S_{\text{BET}}$  and pore volume of 1-a-x/b-SBA-15 also decreased gradually with the increase of grafting capacity (Fig. 4d). The detailed pore structure data is listed in Table 2. Above results indicated that imidazolyl silane was successfully grafted on b-SBA-15, and hybrid organic-inorganic materials can be speedily constructed by mechanochemical methods, without destroying the support.

### 3.2. $\text{CO}_2$ cycloaddition reaction catalyzed by 1-a-x/b-SBA-15

In the initial cycloaddition reaction of  $\text{CO}_2$  and epoxide, 1,2-epoxybutane (EO) was selected as the typical epoxide substrate to investigate the effect of grafting capacity of catalysis 1-a-x/b-SBA-15. As shown in Table 3, when b-SBA-15 alone was used as the catalyst, the reaction cannot be carried out. As expected, all catalysts 1-a-x/b-SBA-15 are active, and 1-a-60/b-SBA-15 achieved the highest yield of 87% under solvent-free conditions. This result indicated that the alkylol-amine cooperative sites in the catalyst are the key to affecting the catalytic

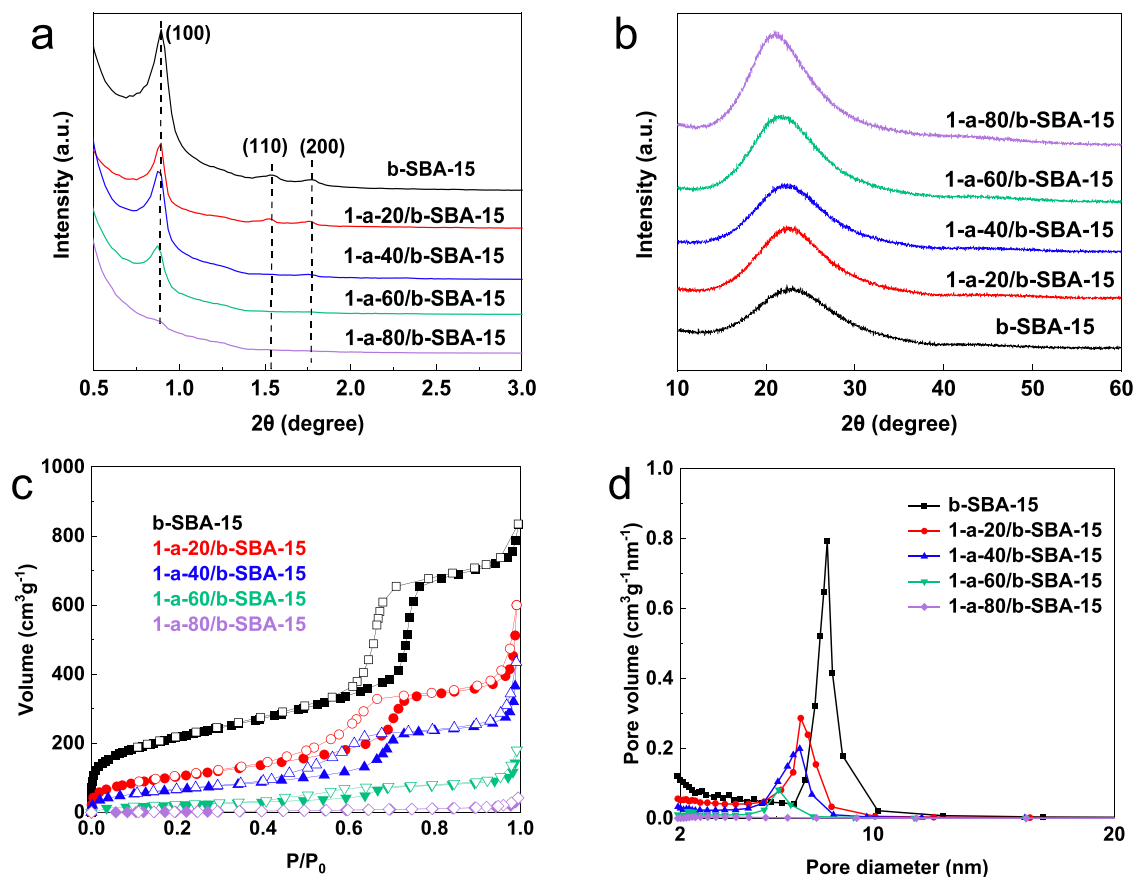


Fig. 4. (a) low-angle XRD patterns, (b) wide-angle XRD patterns, (c) N<sub>2</sub> adsorption-desorption isotherms, and (d) pore size distribution of 1-a-x/b-SBA-15.

Table 2

Effect of grafting capacity of imidazolyl silane on textural property of 1-a-x/b-SBA-15.

Entry	Sample	$S_{\text{BET}}$ (m <sup>2</sup> g <sup>-1</sup> )	Average pore size (nm)	Total pore volume (mLg <sup>-1</sup> )
1	b-SBA-15	767.3	8.1	1.220
2	1-a-20/b-SBA-15	381.6	7.0	0.875
3	1-a-40/b-SBA-15	242.9	6.9	0.644
4	1-a-60/b-SBA-15	83.1	6.1	0.250
5	1-a-80/b-SBA-15	13.9	2.5	0.050

Table 3

Cycloaddition of CO<sub>2</sub> and 1,2-epoxybutane (EO) catalyzed by 1-a-x/b-SBA-15.

Entry	Catalyst	Yield (%) <sup>a</sup>	Selectivity (%) <sup>a</sup>
1	b-SBA-15	0	> 99
2	1-a-20/b-SBA-15	45	> 99
3	1-a-40/b-SBA-15	77	> 99
4	1-a-60/b-SBA-15	87	> 99
5	1-a-80/b-SBA-15	53	> 99

Reaction conditions: EO (10 mmol), catalyst (100 mg), CO<sub>2</sub> (1.0 MPa), 120 °C, 12 h, solvent-free.

<sup>a</sup> Determined by GC-MS.

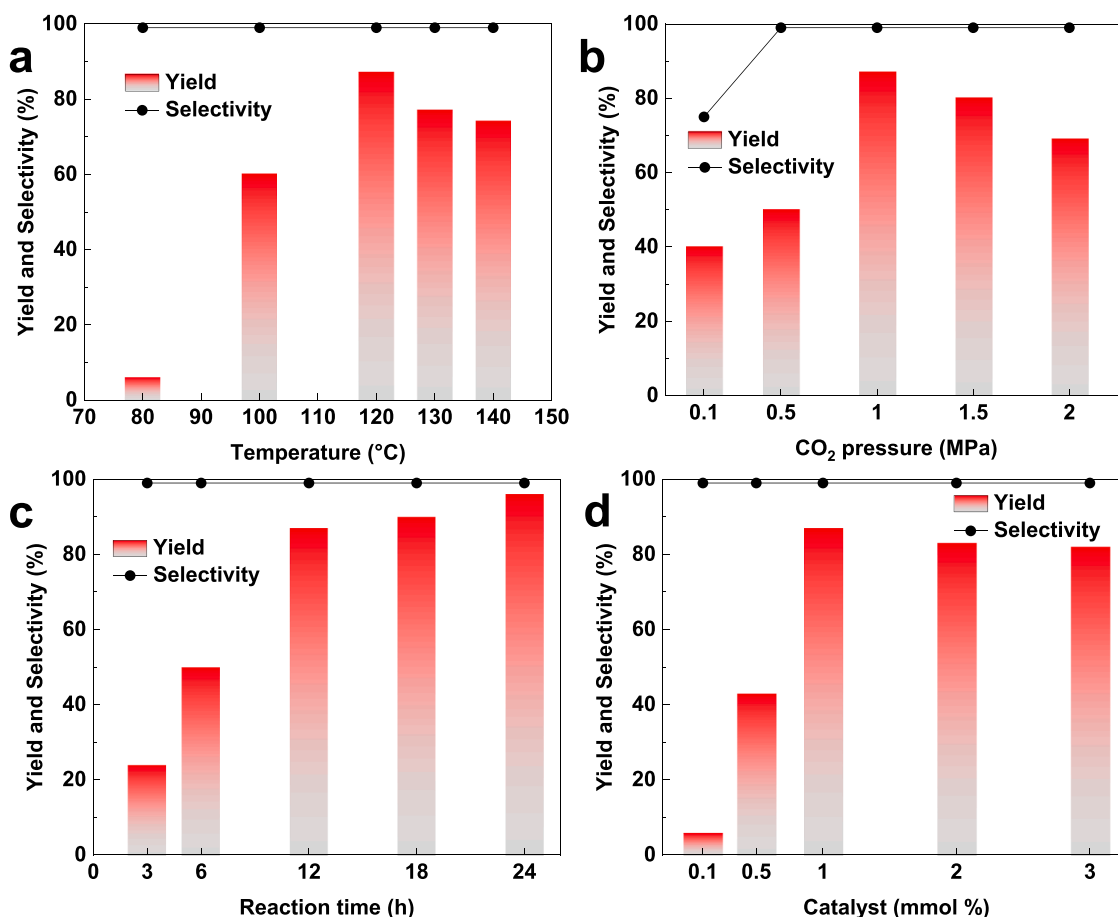
activity of SBA-15 supported catalysts. Compared with most of the catalysts reported in the literature [17,18], the catalyst 1-a-60/b-SBA-15 constructed by mechanochemistry in this paper has achieved considerable yield and excellent selectivity without halogen. Although catalyst

1-a-80/b-SBA-15 has the highest loading capacity, its low reaction activity may be due to the blockage of its pores as described in the previous structural characterization. Therefore, 1-a-60/b-SBA-15 was selected as a candidate catalyst for further studies.

To find out ideal reaction conditions, factors such as reaction time, temperature, CO<sub>2</sub> pressure, and catalyst dosage were investigated, respectively. As shown in Fig. 5a, the yield increased with the reaction temperature, reaching the optimal reaction temperature at 120 °C. With further increasing temperature, the catalyst is slightly deactivated. Meanwhile, the yield increased as CO<sub>2</sub> pressure rose from 0.1 to 1.0 MPa and staid at maximum with a CO<sub>2</sub> pressure of 1.0 MPa (Fig. 5b). It is worth noting that further to increase in pressure are disadvantageous for conversion. We speculated that CO<sub>2</sub> in the reaction mixture is enriched in the pores and decreases in the local epoxides concentration near the active components of catalyst, reducing the interaction between epoxides and catalyst [44]. As the reaction time was prolonged, the yield gradually increased and already exceeded 90% at 18 h (Fig. 5c). The amount of catalyst has a great influence on the reaction, and the yield increased from 6% to 87% with increasing catalyst loading from 0.1 to 1 mol%. The amount of catalyst further provided has no significant change in yield. Finally, 1.0 MPa CO<sub>2</sub>, 1 mol% catalyst loading, 18 h and 120 °C were chosen as appropriate conditions for CO<sub>2</sub> cycloaddition reaction.

With the optimized conditions in hand, epoxides with different terminal substituents were used to study general applicability. It can be seen from Table 4 that the catalyst 1-a-60/b-SBA-15 shows excellent activity for the cycloaddition with moderate to good yields of various cyclic carbonates (60–92%). Notably, the yields of cyclic carbonates decreased with the increase of alkyl chain length for epoxides, presumably because the large size of epoxides with long alkyl chains limited the reaction mass transfer (entries 1–3). The conversion of





**Fig. 5.** Optimization of reaction conditions. Activity of 1-a-60/b-SBA-15 in the cycloaddition reaction of CO<sub>2</sub> and EO (10 mmol). (a) effect of temperature by using 1 mol% of 1-a-60/b-SBA-15, 1.0 MPa CO<sub>2</sub>, and 12 h; (b) effect of CO<sub>2</sub> pressure by using 1 mol% of 1-a-60/b-SBA-15, 120 °C, and 12 h; (c) effect of reaction time by using 1 mol% of 1-a-60/b-SBA-15, 1.0 MPa CO<sub>2</sub>, and 120 °C; (d) effect of catalyst loading by using 1.0 MPa CO<sub>2</sub>, 120 °C, and 12 h.

epibromohydrin and epichlorohydrin was high with up to exceeding 90%, but the selectivity was relatively low (entries 4 and 5). In contrast, internal epoxides showed poor activity due to the high steric hindrance of the  $\beta$ -carbon atom (entry 9), affording an inferior yield of only 27% [17,49].

### 3.3. Effects of catalyst structure on catalytic behaviors

The structure of the carrier and active components of the heterogeneous catalyst together determines its catalytic activity. After proving the relationship between imidazolyl silane loading and catalytic activity, we designed a series of y-SBA-15 supported organocatalysts with different functional groups and pore sizes to explore the effect of the structure on the CO<sub>2</sub> cycloaddition reaction. The synthesis of these catalysts was strictly controlled by the consistency of the method to obtain a similar efficiency of silylation. These catalysts were characterized by nitrogen adsorption desorption curve and thermogravimetry (Fig. 6).

As shown in Fig. 6a, terminal branching and bulky steric structure of organocatalysts greatly determined the  $S_{\text{BET}}$  and  $V_{\text{pore}}$  (Table S2). For instance, the  $S_{\text{BET}}$  of 3-a-60/b-SBA-15 is as high as 234.8 m<sup>2</sup>·g<sup>-1</sup>, but the  $S_{\text{BET}}$  of 2-a-60/b-SBA-15 is only 54.2 m<sup>2</sup>·g<sup>-1</sup>. We speculated that the hydrophobic alkyl chains in 2-a-60/b-SBA-15 repel the hydrophilic SiO<sub>2</sub> surface, so the pore structure was well preserved. However, these supported b-SBA-15 organocatalysts appeared a similar average pore size distribution of about 6.2 nm (Fig. 6b), presumably due to their smaller difference in molecular size (Fig. 7a), indicating that the these organocatalysts loaded on b-SBA-15 had little effect on the pore size. In

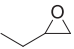
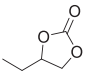

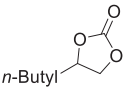
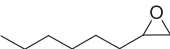
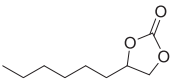
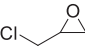
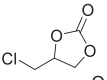
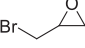
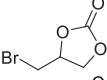
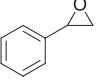
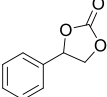
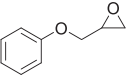
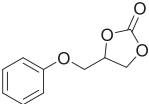
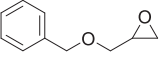
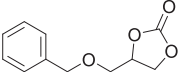
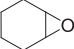
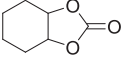
addition, these supported catalysts showed excellent thermal stability (Fig. 6c), which proves that mechanical ball milling can realize the chemical grafting of various silanes.

Three kinds of y-SBA-15 with different pore sizes were used as supports (Structure information are shown in Table S3, Fig. S6 and S7), and the prepared catalysts appeared large differences in specific surface area and average pore sizes (Fig. 6d and e). This structural difference could produce a confined shape-selective catalytic effect. In addition, the pore size difference of the y-SBA-15 had no significant effect on the thermal stability of the catalysts, indicating that the loading mode of 1-a on the y-SBA-15 is consistent. These results demonstrated the better applicability of the mechano-synthesis method for fabricating of the hybrid organic-inorganic SBA-15 supported catalysts with tunable groups and regular pore structures.

Epoxides EO and styrene oxide (SO) with obvious steric differences were selected as substrates to further study the influence of structure on catalytic activity. As shown in Fig. 7b, the 1-a-60/b-SBA-15 with the imidazole group exhibited the highest catalytic activity. This is due to the ability of imidazole to activate CO<sub>2</sub> molecules through the formation of CO<sub>2</sub>-carbene adduct, which has been demonstrated in our previous work [32]. The 2-a-60/b-SBA-15 with a tertiary amine group showed moderate catalytic activity, which may be due to the tertiary amine group promoting the adsorption of CO<sub>2</sub>, thus increasing the concentration of CO<sub>2</sub> in the microenvironment. Indeed, the CO<sub>2</sub> uptake of these SBA-15 supported catalysts also showed that the tertiary amine-functionalized 2-a-60/b-SBA-15 exhibited the highest CO<sub>2</sub> adsorption capacity (Fig. S8a). In addition, the catalyst 3-a-60/b-SBA-15 with an alkyl chain at the end still achieved a moderate yield but slightly



**Table 4**  
Synthesis of various cyclic carbonates catalyzed by 1-a-60/b-SBA-15.

Entry	Substrate	Products	Yield (%)	Selectivity (%)
1			92	> 99
2	<i>n</i> -Butyl 	<i>n</i> -Butyl 	75	> 99
3			60	> 99
4	Cl 	Cl 	89	93
5	Br 	Br 	70	70
6			80	> 99
7			83	91
8			76	92
9			27	> 99

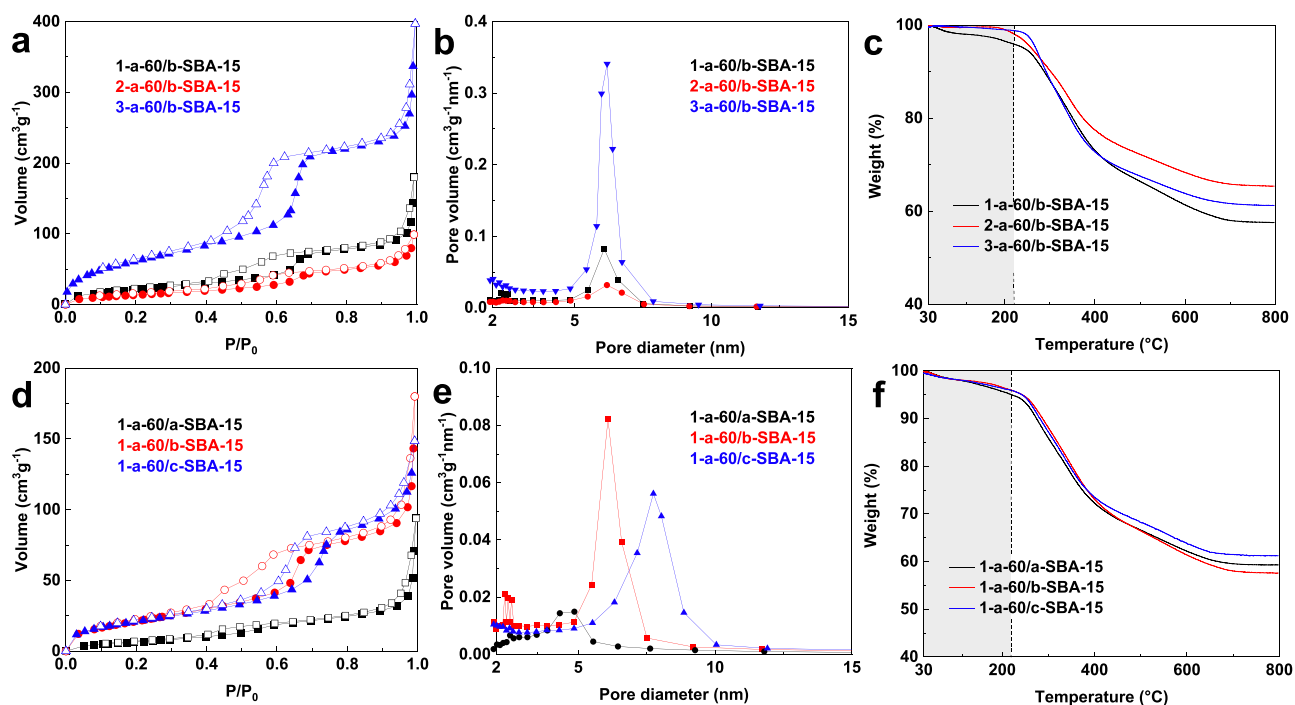


Fig. 6. N<sub>2</sub> adsorption-desorption isotherms (a, d), pore size distribution and (b, e), and TGA curves (c, f) of various n-a-60/y-SBA-15.

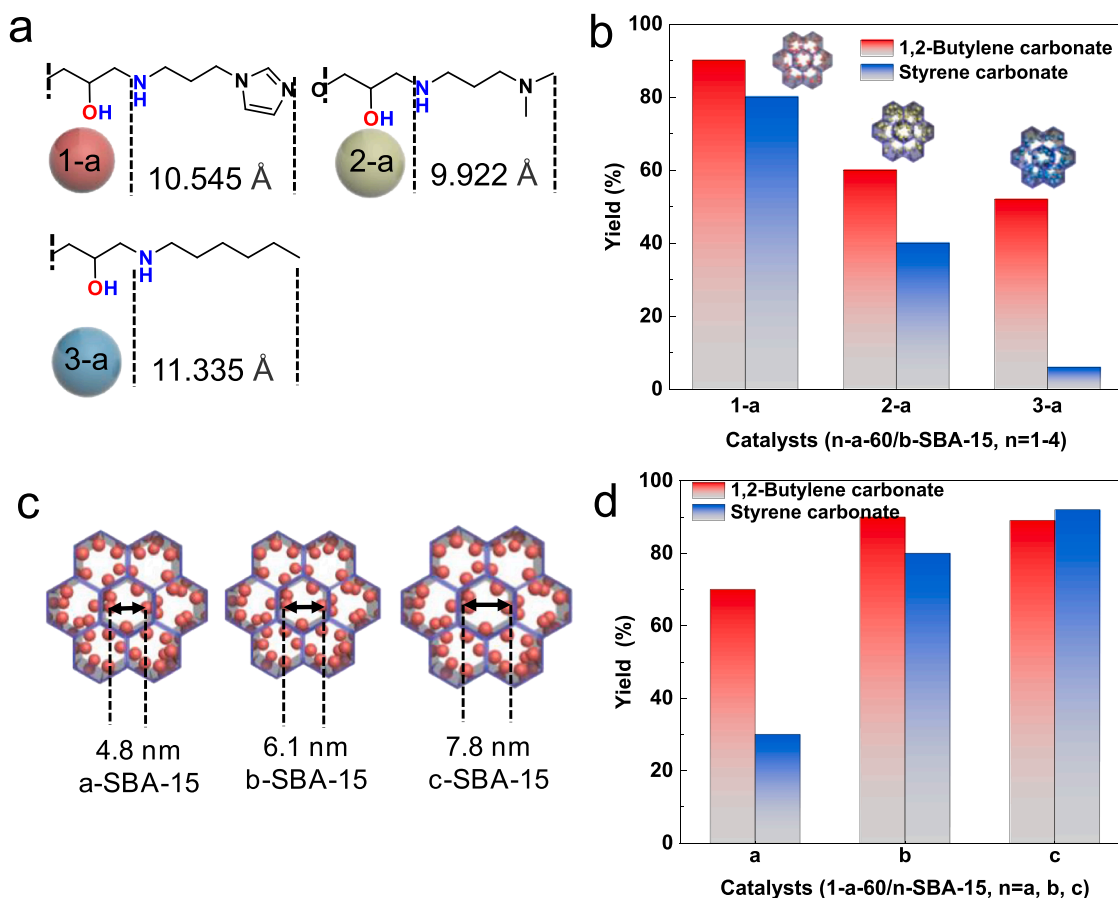


Fig. 7. (a) molecular local dimension of the organocatalysts, (b) effect of different organocatalysts on cycloaddition reaction, (c) average pore size y-SBA-15 after loading 1-a, and (d) effect of average pore size of y-SBA-15 on cycloaddition reaction. Reaction conditions: catalysts (0.5 mol%), substrate (10 mmol), CO<sub>2</sub> (1.0 MPa), 120 °C, and 18 h.

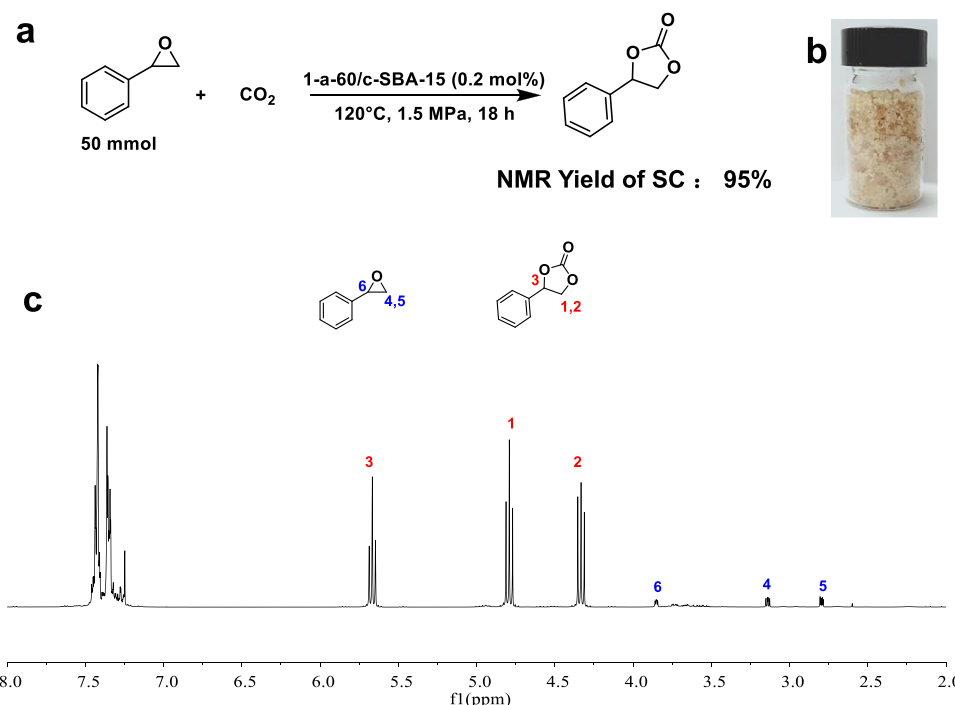


Fig. 8. (a) Schematic diagram of gram-scale synthesis, (b) physical map of product SC, (c)  $^1\text{H}$  NMR of the SC synthesized by gram-scale experiment.

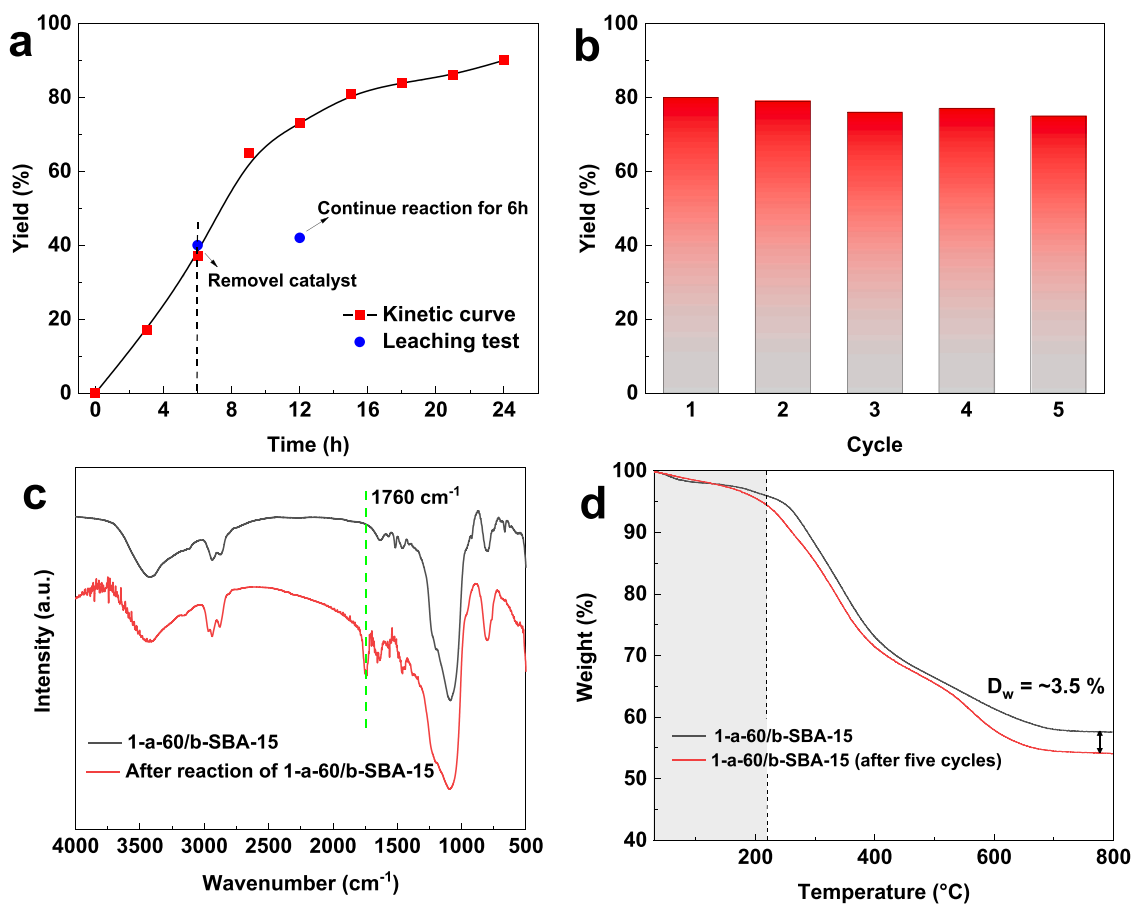
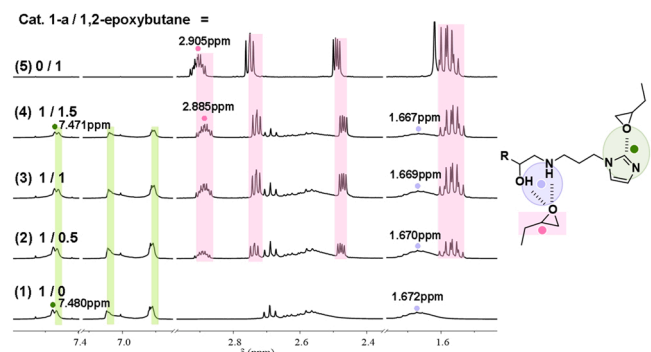
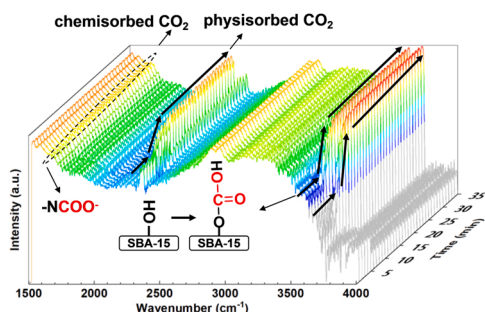


Fig. 9. (a) leaching test for cycloaddition of  $\text{CO}_2$  and SO (10 mmol) catalyzed by 1-a-60/b-SBA-15, (b) recycling catalytic test, (c) FTIR spectra and (d) TGA weight loss profiles of 1-a-60/b-SBA-15 before and after use.

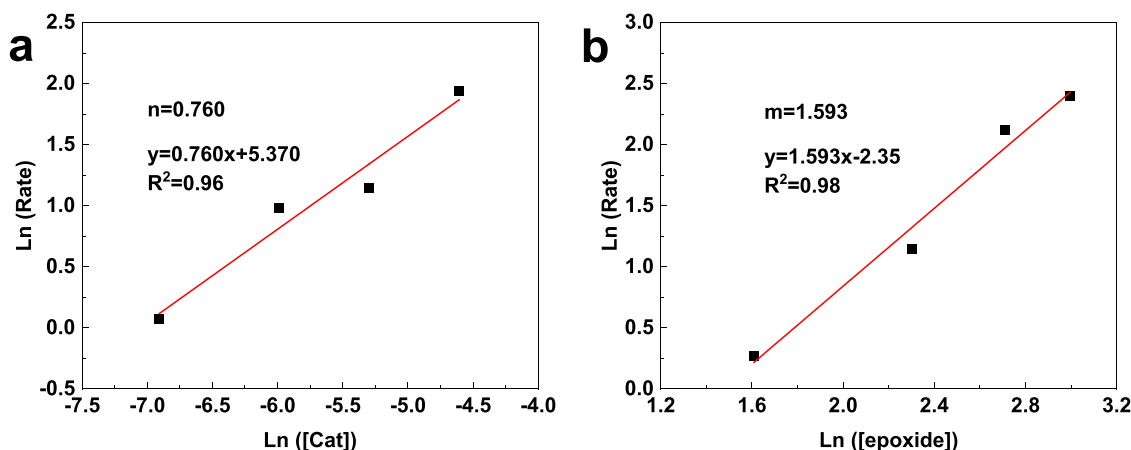


**Fig. 10.** Change in chemical shifts resulting from hydrogen bonding interaction between **1-a** and EO. N-H/O-H (purple), imidazole (green), EO (pink) in the  $^1\text{H}$  NMR spectra, and the mole ratio of **1-a** to EO are (1) 1/0, (2) 1/0.5, (3) 1/1, (4) 1/1.5, and (5) 0/1.

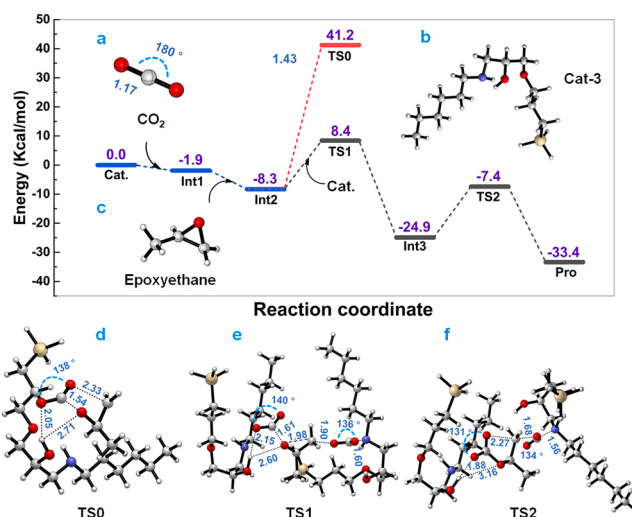


**Fig. 11.** In situ FTIR spectra of  $\text{CO}_2$  adsorption on **1-a-60/b-SBA-15**. Conditions: **1-a-60/b-SBA-15** (50 mg),  $\text{CO}_2$  (0.3 MPa),  $30^\circ\text{C}$  for 35 min.

lower than the **2-a-60/b-SBA-15** with tertiary amine, indicating that the designed alkylol-amine structure is the dominant active center for catalysis. The  $\text{CO}_2$ -TPD was also characterized to further demonstrate the above points (Fig. S8b). Considering the stability of catalyst,  $\text{CO}_2$ -TPD was performed up to  $220^\circ\text{C}$  to examine the basic characteristics of **n-a-60/b-SBA-15**. As results, the temperature range at  $75\text{--}120^\circ\text{C}$  is weak basicity and at  $120\text{--}220^\circ\text{C}$  is medium to strong basicity. The **2-a-60/b-SBA-15** modified by tertiary amine showed the best  $\text{CO}_2$  affinity, which was much higher than that of alkyl chain. Introduction of N functionalities in the hybrid materials can effectively improve the  $\text{CO}_2$  affinity. In particular, imidazole, a group that can both affinity for  $\text{CO}_2$  and activate reactants, showed unexpected catalytic activity.



**Fig. 12.** Logarithmic plots of the initial rate of the cycloaddition of SO with  $\text{CO}_2$  catalyzed by **1-a-60/c-SBA-15** (a) versus catalyst concentrations and (b) versus SO concentrations.



**Fig. 13.** The energy profile (in kcal/mol) for  $\text{CO}_2$  cycloaddition catalyzed by **3-a/SBA-15** and the optimized structures including transition states (bond lengths are given in Å).

The size of the epoxides will also significantly affect the reactivity. This size effect is most significant when using **3-a-60/b-SBA-15** as the catalyst, affording styrene carbonate (SC) only 3% yield. This conversion barrier, which originates from size effects, can be improved by using catalysts with larger pore sizes (Fig. 7c), so that the mass transfer resistance can be effectively reduced. It can be seen from Fig. 7d that the SC yield catalyzed by **1-a-60/a-SBA-15** ( $d = 4.8\text{ nm}$ ) is only 30%, while **1-a-60/c-SBA-15** ( $d = 7.8\text{ nm}$ ) is up to 92%. By reducing the mass transfer resistance of the reaction and the effect of molecular size effects, it is possible to make the yield of SC close to that of EC for catalyst **1-a-60/c-SBA-15**. Noteworthy, the yield of SC was only 47% using equivalent pure **1-a** as a catalyst at the same conditions. The inferior yield was presumed to be due to the poor thermal stability of the **1-a**. It was further confirmed that the catalytic activity of **1-a** can be enhanced by grafting **1-a** onto the mesoporous of SBA-15. The porous structure of the catalyst leads to restrict reactants and catalysts in the same space, increasing the possibility of successful collisions. Comparing with homogeneous reaction, chemical reaction is usually controlled by random collisions based on molecular diffusion [50–52]. It can be seen that and the control of catalytic activity and selectivity by confinement effects is also a brilliantly design in the reaction. The above results provided a useful strategy for regulation of immobilized catalysts to improve catalytic performance.



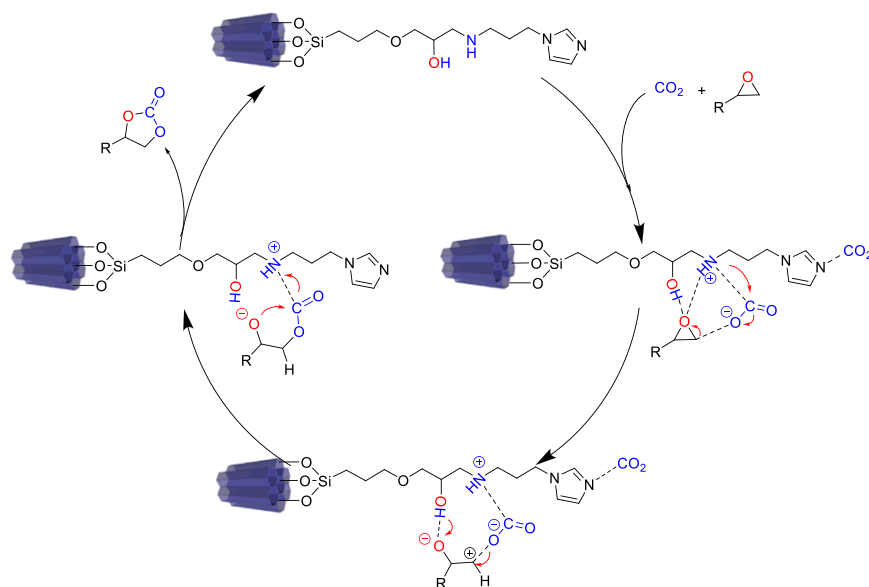


Fig. 14. Proposed mechanism for synthesis of cyclic carbonate catalyzed by 1-a/SBA-15.

### 3.4. Gram-scale synthesis and stability study

To evaluate the application effect of the catalyst, the gram-scale synthesis and catalyst stability were carried out. When the reaction was amplified to 50 mmol, the  $^1\text{H}$  NMR yield of SC reaches 95%, and no by-product was generated (Fig. 8). These results implied that 1-a-60/c-SBA-15 can be used for scale-up synthesis of SC and high-purity products can be prepared. Compared to the halogen-free catalysts reported in the literature (Table S4), the mechanochemically constructed SBA-15 supported organocatalysts (n-a-x/y-SBA-15) with tunable alkylol-amine cooperative sites exhibit better or equivalent  $\text{CO}_2$  conversion performance.

The stability of 1-a-60/b-SBA-15 was demonstrated by the leaching test. After centrifugal separation of the catalyst, the yield barely increased after continuing the reaction for 6 h (Fig. 9a). It was speculated that only a few active components of the catalyst are lost. In addition, the cycle performance of the catalyst was investigated. The activity of the catalyst was found to decrease slightly but still was maintained above 76% (Fig. 9b) after five cycles. In comparing the FTIR spectra of before and after use, a new peak was observed at approximately  $1760\text{ cm}^{-1}$ , which was attributed to the characteristic absorption peak of the cyclic carbonate remaining in the catalyst (Fig. 9c) [8,21]. The TGA analysis of 1-a-60/b-SBA-15 before and after use showed a small amount of residue with about 3.5 wt% (Fig. 9d). For further qualitative analysis, the used catalyst was characterized by XPS. The results showed that the content of C-O bond increases slightly, which is the adsorbed cyclic carbonate (Fig. S9). This is consistent with the conclusion of FTIR. These results indicate that the halogen-free 1-a-60/b-SBA-15 has good stability and excellent catalytic activity in gram-scale reactions, making it an alternative catalyst for  $\text{CO}_2$  fixation into cyclic carbonates.

### 3.5. Study on catalytic mechanism

#### 3.5.1. $^1\text{H}$ NMR titration experiments

$^1\text{H}$  NMR titration experiments were performed to explore the mechanism of the cycloaddition reaction (Fig. 10). After the addition of EO to 1-a, the chemical shifts of the imidazole hydrogen shifted from 7.480 to 7.471 ppm; meanwhile, the methine protons on the epoxide were down-field from 2.885 to 2.905 ppm. The fact suggested the hydrogen bonding interaction between 1-a and EO. In addition, a weak chemical shift of proton also could be observed to shift from 1.672 to

1.667 ppm. It was further confirmed that the intermolecular hydrogen bonding between the 1-a and EO. In particular, relying on the alkylol-amine cooperative sites can facilitate the activation of epoxide molecules.

#### 3.5.2. In situ FTIR study

To further investigate the mechanism, the adsorption behavior of  $\text{CO}_2$  over the 1-a-60/b-SBA-15 surface was also monitored by using in situ FTIR, as shown in Fig. 11. A new peak at  $1715\text{ cm}^{-1}$  was attributed to the stretching vibrations of carbonyl groups in the carbamic acid formed by the adsorption of  $\text{CO}_2$  on the amine groups [53]. Here, 1-a-60/b-SBA-15 activates  $\text{CO}_2$  molecules by chemisorption, and the resulting carbamate acts as a nucleophilic reagent to attack the epoxide molecules and promote ring opening reactions. The intensities of the chemical absorption peaks gradually remained constant after adsorbing  $\text{CO}_2$  for 30 min, implying that the  $\text{CO}_2$  adsorption process was accomplished. Moreover, the peak at  $2340\text{ cm}^{-1}$  gradually increased with  $\text{CO}_2$  adsorption, which is typical  $\text{CO}_2$  physisorption. The bands at  $3580\text{--}3700\text{ cm}^{-1}$  attributed to gas-phase  $\text{CO}_2$  overtones also showed a similar trend in the peak intensities [54,55]. This phenomenon indicated that the SBA-15 surface has produced -OOCOH species [56].

#### 3.5.3. Kinetic studies

In order to further verify the reaction mechanism, the kinetics of the cycloaddition reaction of SC and  $\text{CO}_2$  were performed by using 1-a-60/c-SBA-15 as catalyst due to the best catalytic activity, and the rate equation was defined as [57–59]:

$$r = k[\text{CO}_2]^n[\text{Cat}]^m[\text{epoxide}]^m \quad (1)$$

To determine the order with respect to catalyst, the reaction was carried out with four different catalyst concentrations (Fig. S10). The same method was used to analyze the reaction order of epoxides with four different concentrations of SO (Fig. S11). Additionally, Eq. (1) can be written as Eq. (2) or Eq. (3) [60,61].

$$r = k_{\text{obs}}[\text{epoxide}]^m, \text{ where } k_{\text{obs}} = k[\text{Cat}]^n[\text{CO}_2] \quad (2)$$

$$r = -d[\text{epoxide}]/dt = k_{\text{obs}}[\text{epoxide}] \quad (3)$$

where  $k_{\text{obs}}$  represents the pseudo-first order rate constant for the conversion of epoxide.

The following expression can be obtained.

$$-\ln[\text{epoxide}] = k_{\text{obs}}t \quad (4)$$

To understand the reaction kinetics in the synthesis of SC from CO<sub>2</sub> and SO, the parameters were investigated at different reaction temperatures of 100, 110, 120, and 130 °C. By altering the catalyst concentrations, a catalyst concentration reaction order of 0.760 was obtained from the 1-a-60/c-SBA-15 catalyzed cycloaddition of CO<sub>2</sub> and SO (Fig. 12a). The reaction order between 0 and 1 showed a pseudo first-order dependence on catalyst concentration, suggesting the catalyst activates the epoxides through intramolecular catalysis. The kinetic studies of SO concentration were also performed, and a reaction order of 1.593 was obtained (Fig. 12b). The reaction order indicates that there is a reaction process that activates two molecular epoxides simultaneously during the ring opening process. On the basis of the above results, the kinetic equation can be described as Eq. (5):

$$r = k[\text{CO}_2][\text{Cat}]^{0.760}[\text{epoxide}]^{1.593} \quad (5)$$

The parameters were further investigated at temperatures of 100–130 °C (Fig. S12), and the corresponding kinetic equations, R<sup>2</sup>, reaction rate constant  $k_{\text{obs}}$  and  $\ln k_{\text{obs}}$  were listed in Table S5. The correlation coefficients R<sup>2</sup> were close to 1, indicating that the reaction rate is linear with the concentration of SO and follows a pseudo first-order kinetic reaction.

### 3.5.4. DFT studies

The results of <sup>1</sup>H NMR and in situ FTIR indicated that the synergistic effect between the hydroxyl (-OH) and secondary amine (-NH-) groups promoted the conversion of CO<sub>2</sub>. Immediately, the synergistic catalytic mechanism between hydroxyl and secondary amine groups was discussed by DFT calculations. To simplify the calculation, we chose silica-free 3-a/SBA-15 to simulate the process of catalyzing CO<sub>2</sub> conversion. The bond length and transition state of the structures were further examined by using DFT-based theoretical calculations to further determine the mechanism of the cycloaddition between CO<sub>2</sub> and epoxides. All calculations were performed using the Gaussian 09 program, and the energy profile for CO<sub>2</sub> cycloaddition catalyzed by 3-a/SBA-15 in Fig. 13. During the calculation, silane (-SiH<sub>3</sub>) is used to represent the Si-O bond in the supported carrier (3-a/SBA-15) to allow calculations to be performed within reasonable time periods. The reasonable configurations are shown in Fig. S13.

First, the binding between CO<sub>2</sub> and the N-H group of the catalyst is slightly exothermic (−1.9 kcal/mol) (Int1). When epoxyethane is added, the -OH group on 3-a/SBA-15 serves as hydrogen bond donor (HBD), fixing the oxygen atom on one side of epoxyethane and CO<sub>2</sub> by intermolecular hydrogen bonding, in which their bond lengths are 1.88 and 2.77 Å, respectively (Int2). Because there is no halogen existing to stabilize the secondary carbon on the epoxyethane as in the literature [62], the reaction is problematic due to the energy barrier of the transition state (TS0) is as high as 49.5 kcal/mol. The current reaction, however, was conducted under halogen-free conditions. Thus, it is clear that this pathway makes no sense. As a result, it is discovered that the secondary carbon on epoxyethane can be stabilized by the negative oxygen on CO<sub>2</sub> stabilized by 3-a/SBA-15 (bond length of N-CO<sub>2</sub>: 1.60 Å). In TS1, the C-O bond of epoxyethane is elongated (1.43 vs. 1.98 Å) because of the interaction between the negative oxygen on CO<sub>2</sub> and the secondary carbon on epoxyethane (1.90 Å). The oxygen atom on the epoxyethane is now attacked by another CO<sub>2</sub> molecule, which results in the formation of an intermediate (1.61 vs. 1.40 Å, Int3). The energy barrier of TS1 is only 16.7 kcal/mol, which is roughly a 2/3 reduction compared to TS0, considerably decreasing the reaction energy and making this catalytic reaction more plausible. The final product, cyclic carbonate, is created by cyclization in the TS2 (2.27 vs. 1.35 Å, Pro). This procedure results in the formation of cyclic carbonate and the adduct of CO<sub>2</sub>-3-a/SBA-15 when the oxygen atom on CO<sub>2</sub> attacks the stabilized secondary carbon on epoxyethane. It is reliable that the catalyst 3-a/SBA-15 can catalyze the cycloaddition reaction between CO<sub>2</sub> and epoxides under

halogen-free conditions.

### 3.5.5. Proposed mechanism

On the basis of the above experimental results and previous works [14,63–66], a possible mechanism for the catalytic cycloaddition of CO<sub>2</sub> and epoxide catalyzed by 1-a/SBA-15 was proposed (Fig. 14). First, the -OH and N-H groups on the 1-a/SBA-15 act as HBDs to facilitate epoxide activation through intermolecular hydrogen bonding. Here, the imidazole group as a typical group that promotes activation of epoxides will not be discussed too much. Meanwhile, the N on 1-a/SBA-15 provided Lewis base sites for the adsorption and activation of CO<sub>2</sub>. Then, the oxyanion in the activated CO<sub>2</sub> nucleophilic attacked the C (β site) of the epoxide, synergistically polarizing the C-O bond of the epoxide. Among them, a new C-O bond would be formed, further leading to the formation of the carbonate half-ester intermediate. Finally, the cyclic carbonate was formed by the oxyanion of the epoxide moiety in the carbon half-ester intermediate, which further attacked the C atom of CO<sub>2</sub>.

## 4. Conclusions

In summary, a series of mesoporous silicon-supported organo-catalysts with alkylol-amine cooperative sites were fabricated via a mechanical ball milling strategy under solvent-free and room temperature conditions. These hybrid materials were found to be efficient catalysts for catalytic conversion of CO<sub>2</sub> to cyclic carbonate in moderate to good yields under mild solvent- and halogen-free conditions. Moreover, the catalyst also shows excellent stable circulation performance. The study on the structure-activity relationship showed that the alkylol-amine cooperative sites and pore sizes of SBA-15, as well as the loading of the organocatalysts, are the key factors affecting the activity of the n-a-x/y-SBA-15. Further mechanism studies also provided significant insight into the reaction mechanism, demonstrating a hydrogen-bonding catalytic process after capturing CO<sub>2</sub> over the catalyst. This work not only provides a good idea for the green construction of multifunctional organic-inorganic hybrid materials, but also provides an alternative halogen-free catalyst for CO<sub>2</sub> conversion.

### CRedit authorship contribution statement

**Cheng Li:** Investigation, Writing – original draft. **Wenjie Xiong:** Investigation, Writing – original draft. **Tianxiang Zhao:** Investigation, Conceptualization, Writing – review & editing, Funding acquisition. **Fei Liu:** Investigation, Visualization. **Hesan Cai:** Investigation. **Peng Chen:** Investigation. **Xingbang Hu:** Funding acquisition, Conceptualization.

### Declaration of Competing Interest

The authors declare that they have no known competing financial interests or personal relationships that could have appeared to influence the work reported in this paper.

### Data Availability

Data availability Data will be made available on request.

### Acknowledgment

This work was supported by the National Natural Science Foundation of China (nos. 22168012 and 22208070), Innovation Group Project of Education Department in Guizhou Province (no. 2021010), and Project funded by China Postdoctoral Science Foundation (no. 2022M711551). We also would like to thank the researchers in the Shiyanjia Lab ([www.shiyanjia.com](http://www.shiyanjia.com)) for their helping with TEM and <sup>13</sup>C solid-state NMR analysis.

## Appendix A. Supporting information

Supplementary data associated with this article can be found in the online version at [doi:10.1016/j.apcatb.2022.122217](https://doi.org/10.1016/j.apcatb.2022.122217).

## References

- [1] J.A. James, S. Sung, H. Jeong, O.A. Broesicke, S.P. French, D. Li, J.C. Crittenden, Impacts of combined cooling, heating and power systems, and rainwater harvesting on water demand, carbon dioxide, and NO<sub>x</sub> and TCE emissions for Atlanta, Environ. Sci. Technol. 52 (2018) 3–10.
- [2] A.M. Appel, J.E. Bercaw, A.B. Bocarsly, H. Dobbek, D.L. DuBois, M. Dupuis, J. G. Ferry, E. Fujita, R. Hille, P.J.A. Kenis, C.A. Kerfeld, R.H. Morris, C.H.F. Peden, A. R. Portis, S.W. Ragsdale, T.B. Rauchfuss, J.N.H. Reek, L.C. Seefeldt, R.K. Thauer, G. L. Waldrop, Frontiers, opportunities, and challenges in biochemical and chemical catalysis of CO<sub>2</sub> fixation, Chem. Rev. 113 (2013) 6621–6658.
- [3] T.T. Liu, J. Liang, R. Xu, Y.B. Huang, R. Cao, Salen-Co(III) insertion in multivariate cationic metal-organic frameworks for the enhanced cycloaddition reaction of carbon dioxide, Chem. Commun. 55 (2019) 4063–4066.
- [4] B. Schaeffner, F. Schaeffner, S.P. Verevkin, A. Boerner, Organic carbonates as solvents in synthesis and catalysis, Chem. Rev. 110 (2010) 4554–4581.
- [5] A.A.G. Shaikh, S. Sivaram, Organic carbonates, Chem. Rev. 96 (1996) 951–976.
- [6] K. Naveen, H. Ji, T.S. Kim, D.W. Kim, D.-H. Cho, C<sub>3</sub>-symmetric zinc complexes as sustainable catalysts for transforming carbon dioxide into mono- and multi-cyclic carbonates, Appl. Catal. B Environ. 280 (2021), 119395.
- [7] S. Jayakumar, H. Li, L. Tao, C.Z. Li, L.N. Liu, J. Chen, Q.H. Yang, Cationic Zn-porphyrin immobilized in mesoporous silicas as bifunctional catalyst for CO<sub>2</sub> cycloaddition reaction under cocatalyst free conditions, ACS Sustain. Chem. Eng. 6 (2018) 9237–9245.
- [8] Z.Y. Gao, L. Liang, X. Zhang, P. Xu, J.M. Sun, Facile one-pot synthesis of Zn/Mg-MOF-74 with unsaturated coordination metal centers for efficient CO<sub>2</sub> adsorption and conversion to cyclic carbonates, ACS Appl. Mater. Interfaces 13 (2021) 61334–61345.
- [9] N. Wei, Y. Zhang, L. Liu, Z.B. Han, D.Q. Yuan, Pentanuclear Yb(III) cluster-based metal-organic frameworks as heterogeneous catalysts for CO<sub>2</sub> conversion, Appl. Catal. B Environ. 219 (2017) 603–610.
- [10] W. Xu, H. Chen, K.C. Jie, Z.Z. Yang, T.T. Li, S. Dai, Entropy-driven mechanochemical synthesis of polymeric zeolitic imidazolate frameworks for CO<sub>2</sub> fixation, Angew. Chem. Int. Ed. 58 (2019) 5018–5022.
- [11] S. Yue, P.P. Wang, X.J. Hao, S.L. Zang, Dual amino-functionalized ionic liquids as efficient catalysts for carbonate synthesis from carbon dioxide and epoxide under solvent and cocatalyst-free conditions, J. CO<sub>2</sub> Util. 21 (2017) 238–246.
- [12] H.T. Peng, Q.J. Zhang, Y. M. Wang, H.L. Gao, N. Zhang, J. Zhou, L.J. Zhang, Q. Yang, Q.H. Yang, Z.Y. Lu, Atomically dispersed Lewis acid sites meet poly(ionic liquid)s networks for solvent-free and co-catalyst-free conversion of CO<sub>2</sub> to cyclic carbonates, Appl. Catal. B Environ. 313 (2022), 121436.
- [13] M.D.W. Hussain, A. Giri, A. Patra, Organic nanocages: a promising testbed for catalytic CO<sub>2</sub> conversion, Sustain. Energy Fuels 3 (2019) 2567–2571.
- [14] L.N. Han, S.W. Park, D.W. Park, Silica grafted imidazolium-based ionic liquids: efficient heterogeneous catalysts for chemical fixation of CO<sub>2</sub> to a cyclic carbonate, Energy Environ. Sci. 2 (2009) 1286–1292.
- [15] W.G. Cheng, X. Chen, J. Sun, J.Q. Wang, S.J. Zhang, SBA-15 supported triazolium-based ionic liquids as highly efficient and recyclable catalysts for fixation of CO<sub>2</sub> with epoxides, Catal. Today 200 (2013) 117–124.
- [16] X. Wu, C.T. Chen, Z.Y. Guo, M. North, A.C. Whitwood, Metal- and halide-free catalyst for the synthesis of cyclic carbonates from epoxides and carbon dioxide, ACS Catal. 9 (2019) 1895–1906.
- [17] F. Zhang, S. Bulut, X.J. Shen, M.H. Dong, Y.Y. Wang, X.M. Cheng, H.Z. Liu, B. X. Han, Halogen-free fixation of carbon dioxide into cyclic carbonates via bifunctional organocatalysts, Green. Chem. 23 (2021) 1147–1153.
- [18] R. Khatun, P. Bhanja, R.A. Molla, S. Ghosh, A. Bhaumik, S.K.M. Islam, Functionalized SBA-15 material with grafted -CO<sub>2</sub>H group as an efficient heterogeneous acid catalyst for the fixation of CO<sub>2</sub> on epoxides under atmospheric pressure, Mol. Catal. 434 (2017) 25–31.
- [19] V. Hiremath, A.H. Jadhav, H.Y. Lee, S. Kwon, J.G. Seo, Highly reversible CO<sub>2</sub> capture using amino acid functionalized ionic liquids immobilized on mesoporous silica, Chem. Eng. J. 287 (2016) 602–617.
- [20] C.K. Yang, Y.L. Chen, X. Wang, J.M. Sun, Polymeric ionic liquid with carboxyl anchored on mesoporous silica for efficient fixation of carbon dioxide, J. Colloid Interface Sci. 618 (2022) 44–55.
- [21] D. Liu, G. Li, H.O. Liu, Functionalized MIL-101 with imidazolium-based ionic liquids for the cycloaddition of CO<sub>2</sub> and epoxides under mild condition, Appl. Surf. Sci. 428 (2018) 218–225.
- [22] A.P. Amrute, B. Zibrowius, F. Schueth, Mechanochemical grafting: a solvent-less highly efficient method for the synthesis of hybrid inorganic-organic materials, Chem. Mater. 32 (2020) 4699–4706.
- [23] S. Sun, L.J. Zhao, J.R. Yang, X.Q. Wang, X.Y. Qin, X.H. Qi, F. Shen, Eco-friendly synthesis of SO<sub>3</sub>H-containing solid acid via mechanochemistry for the conversion of carbohydrates to 5-hydroxymethylfurfural, ACS Sustain. Chem. Eng. 8 (2020) 7059–7067.
- [24] A.P. Amrute, J.D. Bellis, M. Felderhoff, F. Scheth, Mechanochemical synthesis of catalytic materials, Chem. Eur. J. 27 (2021) 6819–6847.
- [25] T. Tsuzuki, Mechanochemical synthesis of metal oxide nanoparticles, Commun. Chem. 4 (2021) 143.
- [26] K.J. Ardila-Fierro, J.G. Hernández, Sustainability assessment of mechanochemistry by using the twelve principles of green chemistry, ChemSusChem 14 (2021) 2145–2162.
- [27] B. Yi, H. Zhao, L. Cao, X. Si, Y. Jiang, P. Cheng, Y. Zuo, Y. Zhang, L. Su, Y. Wang, C. K. Tsung, L.Y. Chou, J. Xie, A direct mechanochemical conversion of Pt-doped metal-organic framework-74 from doped metal oxides for CO oxidation, Mater. Today Nano 17 (2022), 100158.
- [28] N. Mukherjee, A. Marczyk, G. Szczepaniak, A. Sytniczuk, A. Kajetanowicz, K. Grela, A gentler touch: synthesis of modern ruthenium olefin metathesis catalysts sustained by mechanical force, ChemCatChem 11 (2019) 5362–5369.
- [29] D.Y. Zhao, J.L. Feng, Q.S. Huo, N. Melosh, G.H. Fredrickson, B.F. Chmelka, G. D. Stucky, Triblock copolymer syntheses of mesoporous silica with periodic 50 to 300 angstrom pores, Science 279 (1998) 548–552.
- [30] X.G. Xu, B. Pejic, C. Heath, M.B. Myers, C. Doherty, Y. Gozukara, C.D. Wood, Polyethylenimine "Snow": an emerging material for efficient carbon removal, ACS Appl. Mater. Interfaces 11 (2019) 26770–26780.
- [31] Q.Y. Yu, Y.H. Liu, Z. Huang, J. Zhang, C.R. Luan, Q.F. Zhang, X.Q. Yu, Bio-reducible polycations from ring-opening polymerization as potential gene delivery vehicles, Org. Biomol. Chem. 14 (2016) 6470–6478.
- [32] T.X. Zhao, X.B. Hu, D.S. Wu, R. Li, G.Q. Yang, Y.T. Wu, Direct synthesis of dimethyl carbonate from CO<sub>2</sub> and methanol at room temperature using imidazolium hydrogen carbonate ionic liquid as recyclable catalyst and dehydrant, ChemSusChem 10 (2017) 2046–2052.
- [33] S. Grimme, S. Ehrlich, L. Goerigk, Effect of the damping function in dispersion corrected density functional theory, J. Comput. Chem. 32 (2011) 1456–1465.
- [34] S. Grimme, S. Ehrlich, L. Goerigk, Effect of the damping function in dispersion corrected density functional theory, J. Comput. Chem. 32 (2011) 1456–1465.
- [35] R. Sure, J. Antony, S. Grimme, Blind prediction of binding affinities for charged supramolecular host-guest systems: achievements and shortcomings of DFT-D3, J. Phys. Chem. B 118 (2014) 3431–3440.
- [36] Z.H. Li, K.M. Su, J. Ren, D.J. Yang, B.W. Cheng, C.K. Kim, X.D. Yao, Direct catalytic conversion of glucose and cellulose, Green. Chem. 20 (2018) 863–872.
- [37] M.J. Frisch, G.W. T. H.B. Schlegel, G.E. Scuseria, M.A. Robb, J.R. Cheeseman, J. A. Montgomery Jr., T. Vreven, K.N. Kudin, J.C. Burant, J.M. Millam, S.S. Iyengar, J. Tomasi, V. Barone, B. Mennucci, M. Cossi, G. Scammani, N. Rega, G.A. Petersson, H. Nakatsuji, M. Hada, M. Ehara, K. Toyota, R. Fukuda, J. Hasegawa, M. Ishida, T. Nakajima, Y. Honda, O. Kitao, H. Nakai, M. Klene, X. Li, J.E. Knox, H. P. Hratchian, J.B. Cross, V. Bakken, C. Adamo, J. Jaramillo, R. Gomperts, R. E. Stratmann, O. Yazyev, A.J. Austin, R. Cammi, C. Pomelli, J. Ochterski, P. Y. Ayala, K. Morokuma, G.A. Voth, P. Salvador, J.J. Dannenberg, V.G. Zakrzewski, S. Dapprich, A.D. Daniels, M.C. Strain, O. Farkas, D.K. Malick, A.D. Rabuck, K. Raghavachari, J.B. Foresman, J.V. Ortiz, Q. Cui, A.G. Baboul, S. Clifford, J. Cioslowski, B.B. Stefanov, G. Liu, A. Liashenko, P. Piskorz, I. Komaromi, R. L. Martin, D.J. Fox, T. Keith, M.A. Al-Laham, C.Y. Peng, A. Nanayakkara, M. Challacombe, P.M.W. Gill, B.G. Johnson, W. Chen, M.W. Wong, C. Gonzalez, J. A. Pople, GAUSSIAN 03, Gaussian, Inc., Pittsburgh, PA, 2009.
- [38] K. Motokura, S.M. Ding, K. Usui, Y.Y. Kong, Enhanced catalysis based on the surface environment of the silica-supported metal complex, ACS Catal. 11 (2021) 11985–12018.
- [39] L. Muniandy, F. Adam, N.R.A. Rahman, E.-P. Ng, Highly selective synthesis of cyclic carbonates via solvent free cycloaddition of CO<sub>2</sub> and epoxides using ionic liquid grafted on rice husk derived MCM-41, Inorg. Chem. Commun. 104 (2019) 1–7.
- [40] J. Li, D.G. Jia, Z.J. Guo, Y.Q. Liu, Y.N. Lyu, Y. Zhou, J. Wang, Imidazolium based porous hypercrosslinked ionic polymers for efficient CO<sub>2</sub> capture and fixation with epoxides, Green Chem. 19 (2017) 2675–2686.
- [41] G. Yang, X. Hu, J. Liang, Q. Huang, J.B. Dou, J.W. Tian, F.J. Deng, M.Y. Liu, X. Y. Zhang, Y. Wei, Surface functionalization of MXene with chitosan through in-situ formation of polyimides and its adsorption properties, J. Hazard. Mater. 419 (2021), 126220.
- [42] Q.-Y. Guo, X.-Y. Yan, W. Zhang, X.-H. Li, Y.S. Xu, S.Q. Dai, Y.C. Liu, B.-X. Zhang, X. Y. Feng, J.F. Yin, D. Han, J.H. Huang, Z.B. Su, T. Liu, M.J. Huang, C.-H. Hsu, S.Z. D. Cheng, Ordered mesoporous silica pyrolyzed from single-source self-assembled organic-inorganic giant surfactants, J. Am. Chem. Soc. 143 (2021) 12935–12942.
- [43] G.F. Andrade, D.C. Ferreira Soares, R.K. de Sousa Almeida, E.M. Barros Sousa, Mesoporous silica SBA-16 functionalized with alkoxy-silane groups: preparation, characterization, and release profile study, J. Nanomater. 2012 (2012), 816496.
- [44] M.S. Liu, P.H. Zhao, R. Ping, F.W. Liu, F.S. Liu, J. Gao, J.M. Sun, Squaramide-derived framework modified periodic mesoporous organosilica: A robust bifunctional platform for CO<sub>2</sub> adsorption and cooperative conversion, Chem. Eng. J. 399 (2020), 125682.
- [45] K. Koner, S. Karak, S. Kandambeth, S. Karak, N. Thomas, L. Leanza, C. Perego, L. Pesce, R. Capelli, M. Moun, M. Bhakar, T.G. Ajithkumar, G.M. Pavan, R. Banerjee, Porous covalent organic nanotubes and their assembly in loops and toroids, Nat. Chem. 14 (2022) 507–514.
- [46] T.M. Lima, V. de Macedo, D.S.A. Silva, W.N. Castelblanco, C.A. Pereira, R. E. Roncolato, M.B. Gawande, R. Zboril, R.S. Varma, E.A. Urquiza-Gonzalez, Molybdenum-promoted cobalt supported on SBA-15: Steam and sulfur dioxide stable catalyst for CO oxidation, Appl. Catal. B Environ. 277 (2020), 119248.
- [47] G. Majano, L. Borchardt, S. Mitchell, V. Valtchev, J. Pérez-Ramírez, Rediscovering zeolite mechanochemistry—a pathway beyond current synthesis and modification boundaries, Micro Mesoporous Mater. 194 (2014) 106–114.
- [48] M.A. Al-Ghouti, D.A. Da'ana, Guidelines for the use and interpretation of adsorption isotherm models: a review, J. Hazard. Mater. 393 (2020), 122383.

- [49] Z.J. Shi, Q. Su, T. Ying, X. Tan, L.L. Deng, L. Dong, W.G. Cheng, Ionic liquids with multiple active sites supported by SBA-15 for catalyzing conversion of CO<sub>2</sub> into cyclic carbonates, *J. CO<sub>2</sub> Util.* 39 (2020), 101162.
- [50] Y.G. Shen, X. Wang, J.M. Lei, S.L. Wang, Y.Q. Hou, X. Hou, Catalytic confinement effects in nanochannels: from biological synthesis to chemical engineering, *Nanoscale Adv.* 4 (2022) 1517–1526.
- [51] J.C.S. Terra, A.R. Martins, F.C.C. Moura, C.C. Weber, A. Moores, Making more with less: confinement effects for more sustainable chemical transformations, *Green. Chem.* 24 (2022) 1404–1438.
- [52] K. Hemmer, M. Cokoja, R.A. Fischer, Exploitation of intrinsic confinement effects of MOFs in catalysis, *ChemCatChem* 13 (2021) 1683–1691.
- [53] C. Xu, Z. Bacsik, N. Hedin, Adsorption of CO<sub>2</sub> on a micro-/mesoporous polyimine modified with tris(2-aminoethyl)amine, *J. Mater. Chem. A* 3 (2015) 16229–16234.
- [54] G.Z. Bai, Y. Han, P.P. Du, Z.Y. Fei, X. Chen, Z.X. Zhang, J.H. Tang, M.F. Cui, Q. Liu, X. Qiao, Polyethylenimine (PEI)-impregnated resin adsorbent with high efficiency and capacity for CO<sub>2</sub> capture from flue gas, *New J. Chem.* 43 (2019) 18345–18354.
- [55] D.X. Qin, D.B. Xie, H.P. Zheng, Z.W. Li, J.H. Tang, Z.J. Wei, In-situ FTIR study of CO<sub>2</sub> adsorption and methanation mechanism over bimetallic catalyst at low temperature, *Catal. Lett.* 151 (2021) 2894–2905.
- [56] X.P. Guo, Z.J. Peng, M.M. Hu, C.C. Zuo, A. Traitangwong, V. Meeyoo, C.S. Li, S. J. Zhang, Highly active Ni-Based catalyst derived from double hydroxides precursor for low temperature CO<sub>2</sub> methanation, *Ind. Eng. Chem. Res.* 57 (2018) 9102–9111.
- [57] B.H. Lv, G.H. Jing, Y.H. Qian, Z.M. Zhou, An efficient absorbent of amine-based amino acid-functionalized ionic liquids for CO<sub>2</sub> capture: High capacity and regeneration ability, *Chem. Eng. J.* 289 (2016) 212–218.
- [58] M.S. Liu, L. Liang, X. Li, X.X. Gao, J.M. Sun, Novel urea derivative-based ionic liquids with dual-functions: CO<sub>2</sub> capture and conversion under metal- and solvent-free conditions, *Green Chem.* 18 (2016) 2851–2863.
- [59] B. Zou, L. Hao, L.Y. Fan, Z.M. Gao, S.L. Chen, H. Li, C.W. Hu, Highly efficient conversion of CO<sub>2</sub> at atmospheric pressure to cyclic carbonates with in situ-generated homogeneous catalysts from a copper-containing coordination polymer, *J. Catal.* 329 (2015) 119–129.
- [60] M.S. Liu, B. Liu, S.F. Zhong, L. Shi, L. Liang, J.M. Sun, Kinetics and mechanistic insight into efficient fixation of CO<sub>2</sub> to epoxides over N-heterocyclic compound/ZnBr<sub>2</sub> catalysts, *Ind. Eng. Chem. Res.* 54 (2015) 633–640.
- [61] Z.X. Yue, M. Pudukudy, S.Y. Chen, Y. Liu, W.B. Zhao, J.Y. Wang, S.Y. Shan, Q. M. Jia, A non-metal Acen-H catalyst for the chemical fixation of CO<sub>2</sub> into cyclic carbonates under solvent- and halide-free mild reaction conditions, *Appl. Catal. A Gen.* 601 (2020), 117646.
- [62] Y.W. Fu, Y.N. X, Z.P. Zeng, A.R. Ibrahim, J. Yang, S.L. Yang, Y.Q. Xie, Y.Z. Hong, Y. Z. Su, H.T. Wang, Y.L. Wang, L. Peng, J. Li, W. L, Mesoporous poly(ionic liquid)s with dual active sites for highly efficient CO<sub>2</sub> conversion, *Green Energy Environ.* (2021), <https://doi.org/10.1016/j.gee.2021.05.013>.
- [63] Z. Fang, R. Ren, Y.Q. Wang, Y. Hu, M.Y. Dong, Z.Z. Ye, Q.G. He, X.S. Peng, Solar-driven all-in-one MOFs-based catalyst for highly efficient CO<sub>2</sub> conversion, *Appl. Catal. B Environ.* 318 (2022), 121878.
- [64] Q. Yi, T.T. Liu, X.B. Wang, Y.Y. Shan, X.Y. Li, M.G. Ding, L.J. Shi, H.B. Zeng, Y. C. Wu, One-step multiple-site integration strategy for CO<sub>2</sub> capture and conversion into cyclic carbonates under atmospheric and cocatalyst/metal/solvent-free conditions, *Appl. Catal. B Environ.* 283 (2021), 119620.
- [65] P. Puthiaraj, S. Ravi, K. Yu, W. Ahn, CO<sub>2</sub> adsorption and conversion into cyclic carbonates over a porous ZnBr<sub>2</sub>-grafted N-heterocyclic carbene-based aromatic polymer, *Appl. Catal. B: Environ.* 251 (2019) 195–205.
- [66] H. Zhou, G.X. Wang, W.Z. Zhang, X.B. Lu, CO<sub>2</sub> adducts of phosphorus ylides: highly active organocatalysts for carbon dioxide transformation, *ACS Catal.* 5 (2015) 6773–6779.